NTNU

Norwegian University of
Science and Technology

Enhancement of the Separation Performances of High Free Volume Polymers for CO_2 Capture

Vilde Stangeland Løining

Chemical Engineering and Biotechnology
Submission date: June 2017
Supervisor: Liyuan Deng, IKP
Co-supervisor: Luca Ansaloni, IKP
Zhongde Dai, IKP

Norwegian University of Science and Technology
Department of Chemical Engineering

Preface

The following Master's Thesis is the last step in finishing a MSc. in Chemical Engineering at Norwegian University of Technology and Science. The thesis is part of the NANOMEMC^2 project, funded by the European Commission.

During the last year, while working with the Specialization Project in the fall of 2016 and the Master's Thesis in the spring of 2017, invaluable help have been provided by the supervisors, Associate Professor Liyuan Deng, Dr. Luca Ansaloni and Dr. Zhongde Dai. A special thank you to Zhongde Dai for always being helpful when stopped in the hallway or approached in the lab/office because I always had *just one more question*!

Spending countless hours in the lab was made better by being there together with Marta Westad Hauge and Natalie Therese Josefson - several fruitful conversations were held here, both academic and non-academic.

Writing my thesis would not have been the same if not for the people sharing my study hall, Marta, Eirik Samuelsen and Åsmund Linga. Thank you for all the good inputs, distractions and good laughs! Not to be forgotten are all the students i Chemistry Building 4, for good conversations, tears of laughter, late night dinners and ice cream breaks!

Abstract

Poly(1-trimethylsilyl-1-propyne) (PTMSP) is a high free volume polymer exhibiting preferable properties such as a very high permeability for application in gas separation. Still, the poor selectivity of PTMSP need to be dealt with before the polymer can be economically and technically viable to utilize. This thesis will focus on creating a mixed matrix membrane by addition of nanoparticles into the polymer phase. The nanoparticles are ZIF-7, ZIF-8 and ZIF-8L which are known to have good properties in relations to gas separation and an affinity for CO_2, and the theory is that the nanoparticles can enhance the separation properties of the membrane. Nanoparticles of titanium dioxide (TiO_2) were also used as fillers.

Analyzes show that the thermal stability of the mixed matrix membranes is good, and that the particles are evenly distributed throughout the membrane matrix when the membranes are fabricated using a casting knife. The solvent used for membrane preparation has proved to be very important. For a pure PTMSP membrane the permeability was reduced by 40% while the separation factor was increased by 150% when changing from chloroform to cyclohexane.

The addition of nanoparticles into the membrane matrix was done with varying results. Only the addition of ZIF-7 increased the separation factor to an extent compared to the linked pure membrane. Overall, the particles were well embedded in the matrix, but did not enhance the separation properties to a great extent. ZIF-8L also showed instability in contact with water vapour.

Sammendrag

Poly(1-trimethylsilyl-1-propyne) (PTMSP) er ett polymer av glassaktig karakter, som har fått mye oppmerksomhet grunnet foretrukne egenskaper som veldig høy permeabilitet innen bruk til gassrensing. PTMSP innehar likevel en dårlig selektivitet som må håndteres før det vil være teknisk og økonomisk gjennomførbart å bruke polymeren til industrielle formål. Denne masteroppgaven fokuserer på å lage en membran bestående av en blanding av organiske og inorganiske stoffer i membran matrisen, ved å tilsette nanopartikler inn i polymerfasen. Nanopartiklene som blir brukt er ZIF-7, ZIF-8 og ZIF-8L, som er porøse partikler som har vist gode egenskaper i sammenheng med gassrensing og en attraksjon til CO_2. Målet er at nanopartiklene skal kunne forbedre separasjonsegenskapene til membranene. I tillegg har uporøse partikler av titan dioksid (TiO_2) blitt brukt som ett additiv.

Analyser viser at den termiske stabiliteten til hybridmembraner er god, og at nanopartiklene har en jevn distribusjon gjennom hele membranen når membranene er lagd ved å benytte en støpe-kniv. Løsemiddelet brukt til å produsere membranene viste seg å ha en stor påvirkning. Permeabiliteten ble redusert med 40% og separasjonsfaktoren økt med 150% når løsemiddelet ble byttet fra kloroform til sykloheksan i en ren PTMSP membran.

Tilsetningen av nanopartikler inn i membranen ble gjort med varierende resultater. Kun tilsats av ZIF-7 økte separasjonsfaktoren sammenlignet med den tilhørende PTMSP membranen. Stort sett ble partiklene godt integrert i polymerfasen, men uten å øke separasjonsegenskapene i stor grad. ZIF-8L viste også ustabilitet i kontakt med vanndamp.

Contents

List of Figures

List of Tables

Nomenclature

Acronyms

CCS Carbon Capture & Storage

CMS Carbon Molecular Sieve

CNT Carbon Nanotubes

DSC Differential Scanning Calorimetry

FT-IR Fourier Transform Infrared Spectroscopy

GC Gas Chromatography

gpu Gas Permeation Unit

KD Kinetic Diameter

MMM Mixed Matrix Membrane

MOF Metal-organic Framework

NP Nanoparticle

PEI Polyethyleneimine

PI Polyimide

PIM Polymer of Intrisic Microporosity

PTMSP Poly(1-trimethylsilyl-1-propyne)

PVA Poly(vinyl alchol)

RH Relative Humidity

TGA Thermogravimetric Analysis

SEM Scanning Electron Microscope

ZIF Zeolitic Imidazolate Framework

Symbols

A Effective Membrane Area

D Diffusion Coefficient

J Gas Flux

L Leaf

P Permeability

p Pressure

$\frac{P}{\ell}$ Permeance

S Solubility Coefficient

$\mathbf{T}_g$ Glass Transition Temperature

w Weight

α Separation Factor

α^{ID} Ideal Selectivity

ℓ Membrane Thickness

Subscripts

d Downstream

i Component i

j Component j

u Upstream

1 Introduction

Over the past decades there has been a great deal of focus on man-made climate change, from both advocates and critics. Amongst scientists and researchers there is a strong consensus that the changes, such as the increasing average temperature on Earth, are due to human activity, and thus a great deal of research and effort have been put into the subject (Falkowski et al., 2000).

Even though the amounts of greenhouse gases in the atmosphere is relatively small, they can have a significant effect on the climate, depending on how much infrared radiation they absorb. Many of the gases also have a long lifetime in the atmosphere, up to as much as 130 years (Wang et al., 1976). Mitigation of greenhouse gases can happen in several different ways, such as switching to less carbon-intensive fuels (e.g. biofuels), and promote renewable energy sources such as wind-, solar-, hydro- and nuclear power and improvement of the biological CO_2 sinks. A considerable effort has been put into greenhouse gas emission by carbon dioxide capture and storage (CCS) as described by Metz et al. (2005) and Gibbins and Chalmers (2008).

CSS is the process of capturing and storing CO_2-emissions from large point sources and storing them in a way so that it will not be released into the atmosphere. Several different methods can be applied to capturing CO_2, e.g. membrane separation, adsorption and absorption. Especially absorption is a widely used method, but the process is expensive and energy-demanding. Gas purification can often happen by combining different capture-methods, depending on what type of molecules the gas consists of, and the requirements to the degree of purity. The purity is often regulated by national and/or international pollution limitations/standards. If the concentration of the species to be separated are high, membrane separation can often be the best choice of separation method. Methods such as absorption and adsorption are more often applied to removal of smaller amounts of pollutants. Membrane separation has achieved an increasing amount of attention, due to the process being more environmentally friendly and having a lower cost and energy consumption than e.g. an absorption process (Deng et al., 2009).

Membranes can be fabricated using either biological or synthetic materials. Membranes made of synthetic materials can be divided further into two different types, inorganic and

organic. Examples of inorganic materials are ceramics, zeolites, glass etc., while organic can be polymers. The better part of fabricated membranes for commercial use are made by organic polymers, but less conventional membrane materials have been formed in the later years (Baker, 2004e). Advantages with polymer materials are that the pure polymer membranes are both easily fabricated and at a low cost (Zhang et al., 2012). One of the disadvantages can be given when comparing the separation properties with the Robeson Upper Bound (Robeson, 2008). The Robeson Upper Bound was first released in 1991, where a number of separation data had been analyzed and an empirical upper limit between the selectivity and permeability was determined for several different gas-pairs. This is based on the trade-off commonly found in polymer membranes, where it is difficult to achieve both high selectivity and permeability simultaneously. The Robeson Upper Bound was updated in 2008, based on new advances within the field. Still, researchers are striving to fabricate membrane materials that are able to "beat" the trade-off given by the Robeson Upper Bound.

The present Master's Thesis is related to improvement of a high free volume polymer, poly(1-trimethylsilyl-1-propyne) (PTMSP). Specifically, the goal is to increase the separation factor of the gas pair CO_2/N_2 without affecting the superpermeable properties of PTMSP to a great extent. This will be done by the fabrication of mixed matrix membranes (MMMs), where inorganic nanoparticles are added into the polymer matrix of PTMSP to improve the selective properties of the membranes. The membranes will be tested for gas permeation and characterised.

2 Theory

The following sections will give a brief introduction to membrane separation theory and some vital materials utilized during the experimental work.

2.1 Membrane Separation

A membrane, illustrated in Figure 2.1, is defined as a discrete, thin interface used to control the permeation of different chemical species in contact with the surface, where specific species are let through the membrane while hindering others. The molecules crossing the membrane are called penetrants. Retentate is the part of the feed that does not cross the membrane, while the permeate is the product obtained on the other side of the membrane. During the last decades membranes have become more important within chemical technology. They are most often used in separation processes, where differences in chemical/mechanical properties of the species are used as a way of separating two or more species. The driving force of the separation process comes from a chemical potential difference across the membrane layer, which can be related either to a difference in pressure, concentration or electrical potential. Even though there has been a major development within membrane separation technology during the last decades, the technology is still considered to be fairly new (Baker, 2004e).

As can be seen in Figure 2.2, there are several different types of membranes. They can be differentiated/classified based on different criteria, but one way is dividing them into groups based on the different separation mechanisms. Convective flow, Knudsen diffusion and molecular sieving are separation mechanisms used for penetrants permeating through porous membranes. The pore size governs which pore flow applies, with the following sizing: convective flow (0.1-10µm) >Knudsen diffusion (20Å-0.1µm) >molecular sieving (5-20Å). When the pore size is in the range of convective flow, the selectivity of the membrane is $\approx$ 1, i.e. there is no selectivity across the membrane surface (Baker, 2004b).

The counterpart to porous membranes are dense membranes. Here the species mainly permeate through the membrane interface by solution-diffusion. The relative transport rates of different species are controlled by the diffusivity and solubility in the membrane material. Diffusivity and solubility are influenced by differences in chemical and/or mechanical

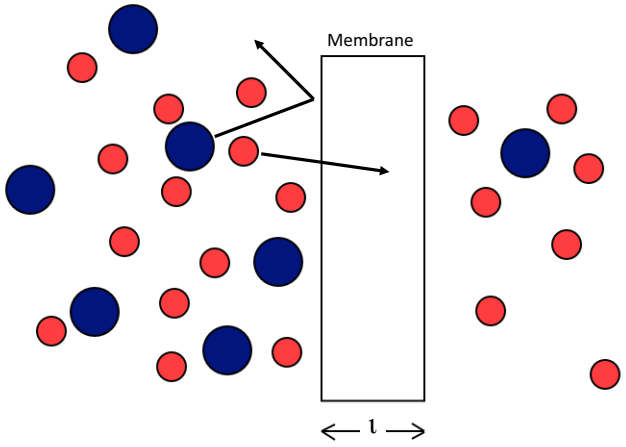

Figure 2.1: Separation of two different species over a membrane.

properties of the penetrating species. Temperature, pressure and species concentration are all factors determining the equilibrium between the membrane material and the permeating fluid at the membrane surface. Once a species has dissolved into the membrane, it diffuses randomly through the membrane and desorbs on the opposite surface. Dense membranes can thus be used to separate species of similar size, such as CO_2 and N_2, due to their difference in chemical properties. The dense membranes are normally used for gas separation, pervaporation and reverse osmosis processes (Baker, 2004c).

As stated previously, the separation mechanisms differ between dense and porous membranes. The relative pore size and permeance of the membrane are important factors related to which separation mechanism applies. The solution-diffusion mechanism is applicable for polymer membranes, which are classified as dense membranes. Due to free volume created by the polymer chains, the penetrants can easily permeate through the membrane matrix. The free volume, often referred to as "empty spaces" within the membrane matrix arises due to thermal motions of the macro-molecules of the polymer, creating temporary pathways for the penetrants through the membrane. It is believed that the molecules/components travel through the membrane by "jumping" between the temporary cavities which are formed by movement in the polymer chain. This is based on simulation models for the solution-diffusion mechanism, and the timescale for the existence of the temporary cavities are believed to be

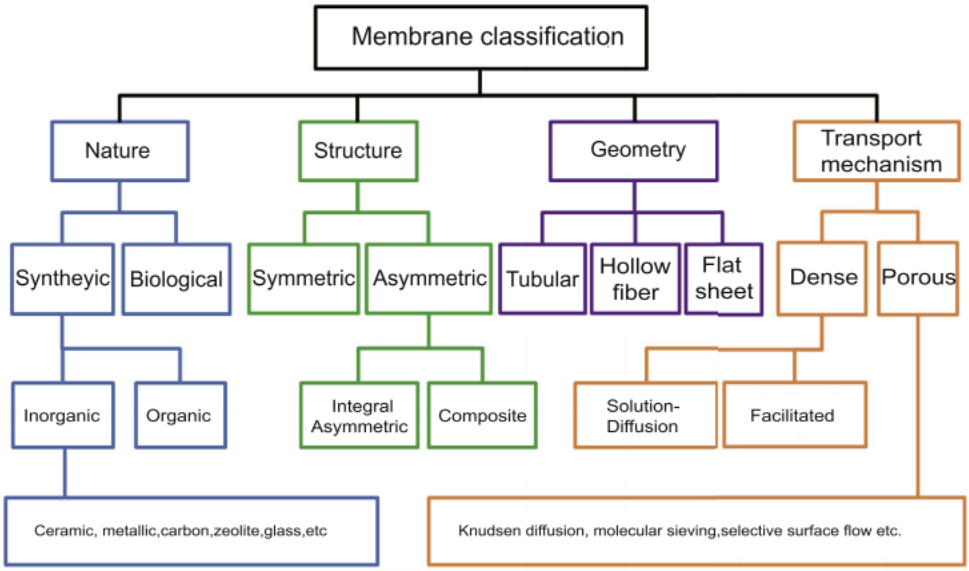

Figure 2.2: Classification of membranes, by Dai et al. (2016).

in the picoseconds (10^{-12}s) (Baker, 2004c).

When free volume elements in a polymer membrane are connected to each other and are relatively large (compared to cavities found in other dense membranes), the transport can have a pore flow characteristic. If the pores/free volume are of a considerable size, the probability of the pores existing more permanently and giving a pore flow characteristic is increased. It is usually differentiated between the two mechanisms (solution-diffusion and pore flow) when the pore diameter is around 5-10 Å (Baker, 2004e,c,b).

When discussing the performance of membranes, there are some properties that are widely used to compare values from experiments and literature. Some of these properties are permeability, permeance, selectivity and separation factor. Permeability is the rate of which a flow goes through a membrane of a specific area and thickness, with the pressure difference over the membrane as the driving force. Permeance is the permeability divided by the membrane thickness, thus it is a measurement of the flow rate of a component through a membrane of given area only, with the pressure difference as the driving force. The selectivity of the membrane describes how well a certain species upstream of the membrane is permeated through the membrane compared to another component. The following equations (2.1-2.4) are used to describe membrane performance. A wide range of units can be used to express permeability and permeance. Equations are given by Baker et al. (2010), Ansaloni and Deng

(2017) and Dai et al. (2016).

$$P_i = D_i S_i = J_i \frac{\ell}{\Delta p A} \tag{2.1}$$

P_i is the permeability, D_i the permeate diffusion coefficient and S_i the solubility coefficient of component i. J_i is the membrane gas flux, ℓ the membrane thickness and A the effective membrane area. Δp is the pressure difference across the membrane. The unit Barrer is a non-SI unit often used in relation with permeability, where 1 Barrer = 10^{-10} $\mathrm{cm^3_{STP}}$·cm/$\mathrm{cm^2}$·s· cmHg. Equation (2.2) gives the permeance of a species over a membrane.

$$\frac{P_i}{\ell} = \frac{D_i S_i}{\ell} = \frac{J_i}{\Delta p A} \tag{2.2}$$

where $\frac{P_i}{\ell}$ is the permeance of the membrane.

The separation factor α_{ij} between two components i and j is given by Equation (2.3).

$$\alpha_{ij} = \frac{y_i / y_j}{x_i / x_j} \tag{2.3}$$

where y (downstream) and x (upstream) represent the molar concentrations of components i and j. The ideal selectivity α^{ID} of the membrane gives a comparison of the permeability/permeance of two components i and j, seeing which components can more easily permeate through the membrane, and is given by Equation (2.4). If $\alpha^{ID}_{ij} = 1$, the permeability of species i and j are equal, if $\alpha^{ID}_{ij} > 1$, then $P_i > P_j$.

$$\alpha^{ID}_{ij} = \frac{P_i}{P_j} \tag{2.4}$$

The separation factor α is more dependent on operating conditions, e.g. upstream and downstream pressure, than the ideal selectivity α^{ID}. When the difference between upstream and downstream partial pressure becomes immense, e.g. when the upstream pressure is very high, or downstream pressure is close to zero, $\alpha \approx \alpha^{ID}$, as given by Equation (2.5) (Dai et al., 2016).

$$\alpha_{i,j} = \frac{y_i/y_j}{x_i/x_j} = \frac{1}{x_i/x_j}\frac{P_i}{P_j}\frac{p_{u,i} - p_{d,i}}{p_{u,j} - p_{d,j}} \approx \frac{P_i}{P_j} = \alpha^{ID} \tag{2.5}$$

From Equation (2.1) the permeability P_i is expressed by $D_i S_i$, where the diffusion coefficient D_i and solubility coefficient S_i are two important factors affecting the selectivity of the membranes. $\frac{D_i}{D_j}$ is defined as the mobility-selectivity for two components i and j, where the diffusion coefficient reflects the molecule's mobility within the membrane. The larger the molecules, the smaller the diffusion coefficient - especially in polymer membranes. This is explained by the fact that larger molecules interact more with the chains in the polymers, and thereby are more hindered than smaller molecules. For polymer membranes, the mobility-selectivity will therefore always favour the transport of smaller molecules. It is important to note that the mobility-selectivity trends are greatly different, if the polymers are glassy or rubbery, depending on if the material is below or above the glass transition temperature T_g. Above T_g the material is rubbery, meaning the material is soft and elastic due to thermal motion/rotation around the chain backbone in the polymer. Below T_g, the material is rigid and tough, due to steric hindrance making thermal motion difficult. When heating a glassy polymer towards T_g, the energy increases to the point where the steric hindrance is overcome, and the material turns rubbery. For glassy polymers, the mobility decreases faster compared with molecule size, due to its more rigid structure (Baker, 2004b).

The solubility-selectivity is defined as $\frac{S_i}{S_j}$, where the solubility coefficient is a value given to describe the energy required for a molecule to be sorbed onto the polymer membrane, greatly dependent on the condensability of the component. The condensability is usually higher for larger molecules, and so is the solubility coefficient. The relation between mobility- and solubility-selectivity and its effect on the overall selectivity is dependent on what type of polymer is used, mainly glassy or rubbery. For glassy polymers, the mobility-selectivity is usually dominant, and thus smaller molecules usually permeate more easily through the membranes (Baker, 2004b).

It is essential to differentiate between a polymer's free volume and the unoccupied volume of a polymer, as represented by figures 2.3 and 2.4. The free volume arises due to oscillations of the atoms, which can create free volume in addition to the unoccupied volume. The free volume of a polymer will fluctuate in correlation with the oscillations of the material and the magnitude of oscillations will increase with an increase in temperature. Fox and Flory

(Painter and Coleman, 1997) had the idea that the critical free volume can be connected to T_g; when the polymer is below T_g, the molecules can no longer move relative to one another.

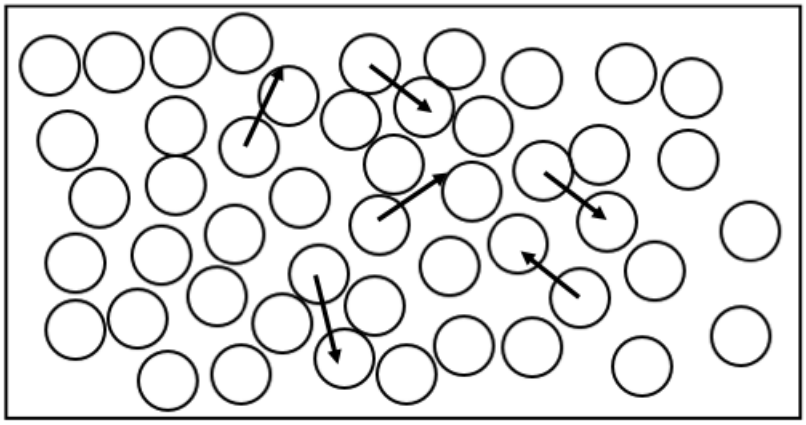

Figure 2.3: Schematic visualization of free volume allowing local translational motion, illustrated by Painter and Coleman (1997).

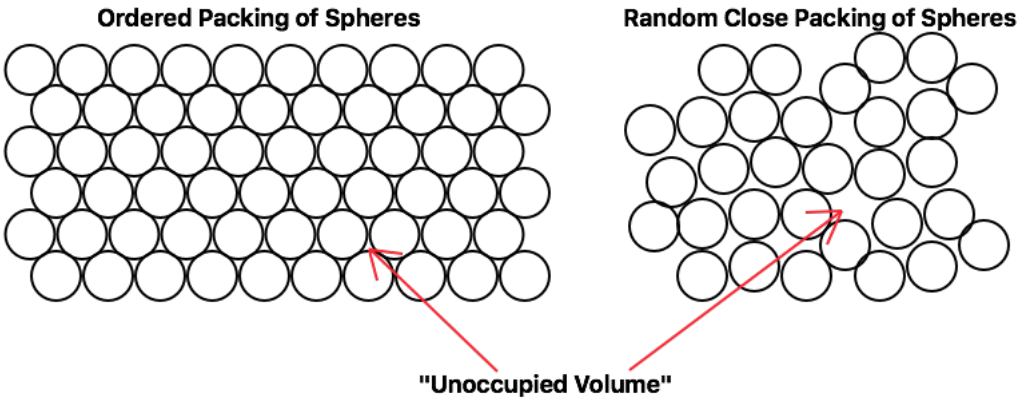

Figure 2.4: Two-dimensional packing of spheres, illustrated by Painter and Coleman (1997).

The free volume of a polymer can be connected to the permeability through a given polymer membrane, where the permeability increases proportionally with an increase in fractional free volume in the polymer. Thus, the transport rate of a penetrant through the membrane will go down over time along with the aging of the polymer.

One of the issues with polymers with high free volume is the rapid aging and the subsequent decrease in permeability. Physical aging in polymers happens by a relaxation of the free volume. This is because glassy polymers are reported to be far from a thermodynamic

equilibrium, especially in the properties of volume, enthalpy and entropy. The difference in the properties compared to the equilibrium state is the driving force that leads to the spontaneous relaxation of the material so that it can come closer to the thermodynamic equilibrium (Ansaloni, 2014).

2.2 Mixed Matrix Membranes

Hybrid membranes are membranes that contain an organic and an inorganic phase. The membranes consist of an organic polymer phase with inorganic fillers embedded in the matrix. One subgroup of this type of membranes is the mixed matrix membrane (MMM). In MMMs, molecular sieving units are dispersed in a polymer phase in order to improve the membrane properties. Reasons for including inorganic fillers are to improve the selectivity and permeability of the membrane, while it also could be promising for decreasing the aging rate of polymer membranes. Choosing fillers based on chemical properties gives rise to easily tuned polymer membranes with uncomplicated processability. The fillers can possess certain properties to tailor membranes for a specific use, but the effect on the transport properties can be either positive or negative, depending on the permeable properties of the fillers. For impermeable fillers, the effect can be negative, where the diffusion of penetrants is reduced, but in varying degree based on molecule size, so the overall separation factor increases. This is due to an increased diffusion pathway within the membrane. For permeable fillers, such as ZIFs (zeolitic imidazolate framework), the polymer and fillers achieve a symbiotic effect where they can work together to increase both the permeability and the separation factor of the membranes. Making MMMs is also desirable from an economic perspective. By coupling a more expensive, high performance nanoparticle with a low-cost polymer the overall cost of membranes is considerably reduced (Ansaloni and Deng, 2016).

The fillers work as molecular sieves in the polymer matrix, and the size of the molecular sieves determines the separation factor between different molecules. Thus, the separation of different compounds can be tailored by choosing a molecular sieve in the size range between the components one wish to separate.

In a MMM it is important to achieve a defect-free membrane, as only one hole in the membrane can highly affect the selectivity. Voids can for example arise if there is not

sufficient adhesion between polymer and filler phase (Mahajan et al., 1999; Ansaloni and Deng, 2016).

2.3 Polymer Phase

As mentioned earlier, most membranes for commercial use are made using polymers, with advantages such as easy fabrication and a low cost. A fair amount of research has been put into the subject of polymers for gas separation. It can be quite complex to choose a polymer for a certain membrane application. The first factor to evaluate are the permeability and selectivity of the membrane in relations to what is to be separated. Other things to keep in mind are the durability and mechanical strength of the membrane under the given operating conditions (Hägg and Deng, 2015).

A wide range of polymers are found to have preferable properties in relations to CO_2 separation. A new type of polymeric materials are the polymerized ionic liquids (PILs) made from ionic liquid monomers. The material present promise within gas separation applications. Polymers of intrisic microporosity (PIM) are a group of polymers with high free volume. The polymers can produce membranes with notable permeability and selectivity. Other interesting polymers are the polyimides (PI), which are attractive due to their availability, a favourable chemical stability and having an easy process of synthesis. The glassy nature of PIs can lead to suitable selectivity for gas separation. Amine based hydrophilic properties are also in focus, with polymers such as poly(vinyl alcohol), poly(vinyl amine) and poly(allyl amine), with their promising properties related to CO_2 capture (Ansaloni and Deng, 2017).

The work in the current thesis is related to the enhancement of separation properties of high free volume polymers, mainly PTMSP, but some work has also been performed with PI. The polymers will be discussed in detail in the following sections.

2.3.1 PTMSP

In Figure 2.5 the chemical structure of the monomer of PTMSP is given. The polymer is a high free volume glassy polymer, and exhibit great promise in making membranes with a very high permeability. Thus, a great deal of effort have been put into research connected

to membrane separation with PTMSP, and the polymer is often referred to as "superpermeable". The high permeability is contributed to the free volume of the polymer, and Wang et al. (2004) and Budd et al. (2004) report the fractional free volume of PTMSP to be approximately 0.30 - 0.34, which is much higher than that of other conventional glassy polymers. The permeability is reported to be in the range of 18000-35200 Barrer for CO_2 and 1500-6745 Barrer for N_2 in literature such as Chapala et al. (2015) and Srinivasan et al. (1994). The considerable range of reported permeability can have several explanations; different preparation/casting conditions, different solvents and the age of the membrane are some of the reasons that can contribute. Budd et al. (2004) report PTMSP membranes to be "microporous" due to the high free volume, even though it is classified as a dense membrane. The interconnected free volume of the membrane is believed to contribute to a rapid diffusion of gas through the membrane, thus leading to the exceptionally high permeability of the membrane, as described by Budd et al. (2004).

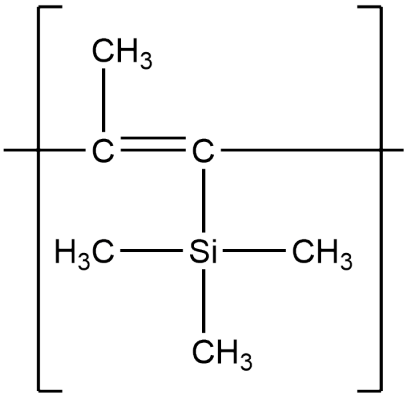

Figure 2.5: Chemical structure of PTMSP.

Even though PTMSP is an especially promising for fabrication of membranes, there are still concerns that need to be tackled. The polymer demonstrates a rapid aging-effect due to relaxation of the free volume. The relaxation in turn decreases the flux through the membrane. The selectivity of the membrane also makes the pure polymer unsuitable for industrial use, as it is not good enough in its pure form. Low et al. (2013) reported that the CO_2/N_2 selectivity should be at least 20-100 for the membrane to be attractive in post-combustion CCS. Bazhenov et al. (2016) reports the selectivity of pure PTMSP membranes that have been cross-linked to be around 4-5 for CO_2/N_2, with a slight increase as the permeability of the membrane is reduced due to aging.

2.3.2 Polyimide (PI)

PIs are polymers created by reaction between an organic (di)anhydride and a diamine (Gooch, 2007). Especially the aromatic group of PIs are gaining a lot of attention due to their excellent properties, such as mechanical strength, chemical resistance, a very high thermal stability and a rigid structure. The easy fabrication process and commercial availability of the glassy polymer also contributes to making it a suitable prospect for membrane-applications as well as for organic solvent nanofiltration (OSN) (Ansaloni and Deng, 2016). PI membranes show great promise, as they not only have good chemical properties, but also show a high selectivity for separation of certain species, such as O_2/N_2 and CO_2/CH_4. The good performance of PI membranes for use in gas separation have been documented to be due to the chemical structure of the polymer, the fractional free volume and the degree of crystallinity. The species to be separated also makes an impact on the membrane performance. Several studies have been performed trying to improve the permeability and selectivity of PI membranes. Some of the actions that have been taken in trying to improve the properties are thermal treatment and both UV- and chemical cross-linking of the membrane. Especially the chemical cross-linking of the polymer present good results, where the choice of cross-linking agent will affect the performance significantly (Shao et al., 2008).

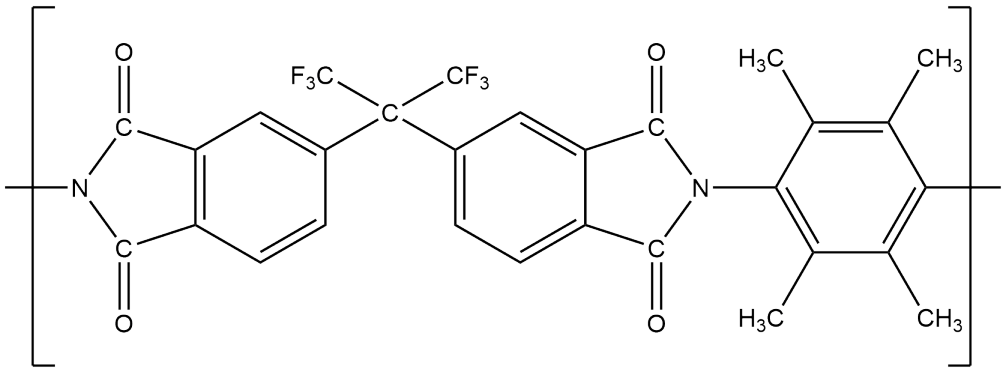

Figure 2.6: Chemical structure of 6FDA-durene.

4,4-(hexafluoroisopropylidene) diphthalic anhydride (6FDA) is a dianhydride used in manufacturing of PIs. Several polyimides made with 6FDA have been reported to have both high selectivity and gas permeability, making it interesting in use for gas separation. As with other high free volume polymers such as PTMSP, polyimides made with 6FDA also show signs of rapid aging with a subsequent decay in permeability. For the gas-pair CO_2/CH_4

6FDA-durene shows a selectivity of 20 at 2 atm and 35°C. The permeability of CO_2 and N_2 is reported to be 677 and 38 Barrer, respectively, at the same conditions. After 280 days, a 6FDA-durene membrane showed between 22-42% decay in permeability of different gasses (He, H_2, O_2, N_2,CH_4 and CO_2), where the decrease was proportional with the size of the gas molecules. For the larger molecules, the decrease was more substantial. This decrease in permeability was also reported for other 6FDA-polyimide membranes, such as 6FDA-DAF and 6FDA-IPDA. The loss of permeability is likely believed to be due to a decrease in the excess free volume of the polymers over time (Lin and Chung, 2001). The chemical structure of 6FDA-durene is given by Figure 2.6.

2.4 Nanoparticles

Nanoparticles are defined as particles with at least one dimension in the nanometer-range. As mentioned earlier, incorporating inorganic fillers in an organic membrane could greatly increase the separation properties. A great amount of research has been put into the subject, and there are a number of possible fillers. Carbon molecular sieves (CMS) demonstrate a good affinity towards glassy polymers, but has a disadvantage of issues concerning achieving a defect-free membrane. Most likely the majority of hybrid inorganic-organic membranes are created with zeolites. Zeolites exhibit a pore size range of 4-10 Å, which is preferable in gas separation and reverse osmosis. The particles can successfully be embedded in rubbery polymers, but there is difficulty related to creating a defect-free interface between particle and glassy polymers. This can greatly reduce the selectivity of hybrid membranes. Another interesting filler is the carbon nanotubes (CNT). CNT's can both enhance transport properties and the mechanical strength of the membrane, but a poor compatibility is present between CNT and polymer phase. Creating defect-free CNT-polymer membranes are a challenging and complicated process, and if not done right the preferable effect of the addition of CNT is greatly weakened. Another group of particles receiving an increasing amount of attention are the metal-organic frameworks (MOFs). MOFs are easily tuned and exhibit a nanopore structure making them interesting for gas separation. MOFs consist of an organic linker and metal subunit. A highly interesting subgroup of MOFs are ZIFs, which display good properties related to molecular sieving. These will be further discussed in relations to CO_2 capture later on. Of impermeable fillers, metal oxides are widely used in nanocom-

posite membranes (NCM). Both titanium and silver oxides show antifouling properties, and are used in water purification. A titanium dioxide (TiO_2) hybrid membrane have also been successfully applied in gas separation.

Different ZIFs are highly interesting due to their exceptional chemical, thermal and hydrothermal stability (Li et al., 2010). Due to these superior properties, ZIFs are excellent for use in molecular sieve membranes. To achieve the best possible performance, it is important that fillers such as ZIFs are similar to the polymer they are to form a mixed matrix with, to obtain a good interface between polymer and filler (Bushell et al., 2013). Since ZIFs have organic part linkers between the metal subunits, the adhesion between polymer and particle are often good. As told by Ansaloni and Deng (2016) and Li et al. (2013), a usual problem can be the cavities formed by a lacking connection at the interface between polymer and nanoparticles as a result of poor adhesion between the two phases. These cavities, illustrated in Figure 2.7, can in turn lead to a highly affected selectivity of the membranes, as the penetrants can take "shortcuts" around the nanoparticles. An additional characteristic to keep in mind when choosing polymer and filler, is that their transport properties should match up to achieve the best possible results. Both the filler and polymer should for example favour transport of either smaller or larger molecules, determined by their solubility and diffusivity (Li et al., 2013).

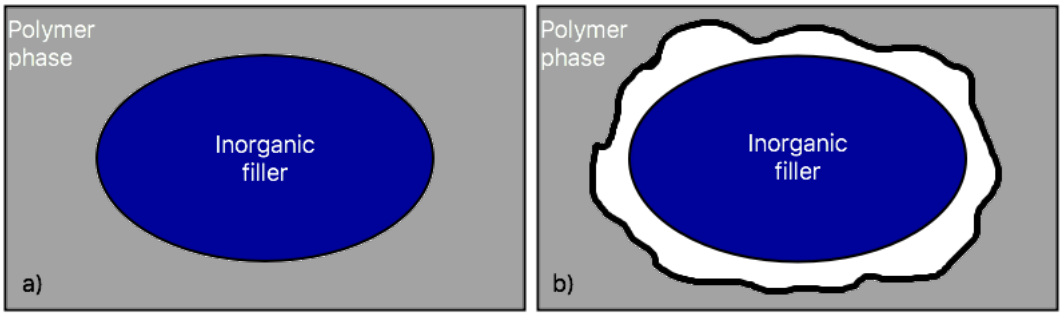

Figure 2.7: Polymer-filler interface in MMM. a) Ideal case of adhesion between polymer and filler, b) interfacial void between polymer and filler. Figure based on Ansaloni and Deng (2016)

ZIFs are 3-D structures with a tetrahedral framework and a pore aperture of 0.2-1.5 nm (2-15 Å). They are built up by inorganic metal ions forming the tetrahedral environment with imidazolate ligand-bridges. The properties of the ZIFs can be tuned by using different

imidazolate-units, where the porous structure and topology of the particles can be affected. The conditions for synthesis can also affect the crystallization of the particles, where size, morphology and topology can be tuned. In relation with the global efforts to reduce CO_2-emissions, ZIFs have been widely studied as adsorbents used in CO_2-capture. They work well as adsorbent for CO_2 due to the possibility of creating particles with large "cages"/cavities and smaller pore aperture, so that they can be size-selective and trap molecules within the structure (Chen et al., 2013).

Research has shown that the addition of different kinds of ZIFs can improve the permeability of mixed matrix membranes, sometimes coupled with an increase in selectivity as well. Some potential uses for ZIF-particles are gas storage, separation processes and use in chemical sensors (Li et al., 2013).

Table 2.1: Kinetic Diameter of Gases (Freeman, 1999).

Gas	**KD** [Å]
H_2	2.8
CO_2	3.3
O_2	3.47
N_2	3.64
CH_4	3.87

Some promising ZIFs are ZIF-8, ZIF-7 and ZIF-8L. ZIF-8 and ZIF-7 have a sodalite topology, giving them special diffusion pathways, which make them interesting for membrane applications. The ZIF's chemical structure are given in figures 2.8-2.10. The kinetic diameter (KD) of ZIF-8 has a pore size of 3.4 Å, while the cavity diameter is 11.6 Å (Bushell et al., 2013). The pore KD is right in between the size of CO_2 and N_2/CH_4, as can be seen in Table 2.1. This makes the nanoparticles perfect for separating CO_2 from the other gases, since the larger molecules will be hindered by their size. Due to the aforementioned large cavities within ZIF-8, the diffusion of molecules through the particles happens quite rapidly. Smaller molecules such as CO_2 and H_2, move through the particles by Knudsen diffusion (Bushell et al., 2013).

Bushell et al. (2013) have performed experimental work where ZIF-8 have been used as a filler in PIM-1, with up to 43wt% nanoparticles in polymer. It was found that the permeability of the gases with smaller molecular size (such as H_2, He and O_2) have a larger increase than the bigger molecules (N_2, CO_2 and CH_4). PIM-1 membranes containing ZIF-8 was found

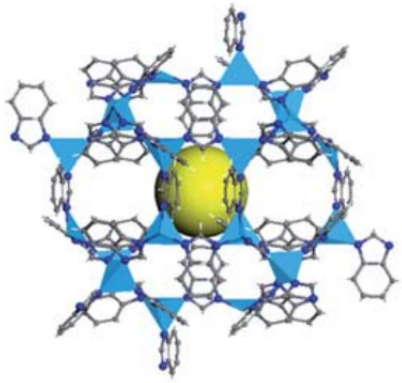

Figure 2.8: Chemical structure of ZIF-7, by Yang et al. (2011).

to have an increase in the free volume, and also a growth in connectivity between the free volume cavities. This could be related to the overall increase of permeability and selectivity of the MMMs.

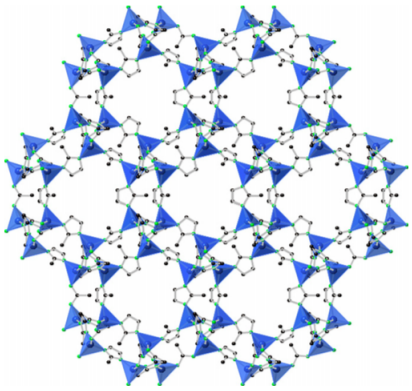

Figure 2.9: Chemical structure of ZIF-8, by Bushell et al. (2013).

While ZIF-8 has a cubic symmetry, ZIF-7 has a hexagonal symmetry. The pore size KD of ZIF-7 is 3 Å, making it useful for separating between smaller molecules such as H_2 and CO_2 (Li et al., 2010). ZIF-7 is particularly interesting in relation to CO_2-separation, as it favours the transport of CO_2 over N_2 and CH_4 due to its higher diffusivity (Li et al., 2013). Even though the pore aperture of ZIF-7 is found to be smaller than the KD of CO_2, there is an induced rotation in the pore-ring, allowing larger molecules to permeate through. The rotation is induced by guest molecules and is made by an organic linker at specific threshold pressures, making the pore-openings very flexible. Another interesting ZIF is the two-dimensional ZIF-8L, where the L stands for leaf. The particle have unique cushion-

shaped cavities, and a leaf-like crystal morphology. The particles exhibit great potential, due to its high pressure stability along with good CO_2-adsorption properties. ZIF-8L is made up of the same building-blocks as ZIF-8, but with a different topology. ZIF-8L particles can be quite big, with dimensions 5 µm x 2 µm x 150 nm. The cavities in the particles are with dimensions 9.4 Å x 7.0 Å x 5.3 Å, and are well suited to accommodate CO_2-molecules (Chen et al., 2013).

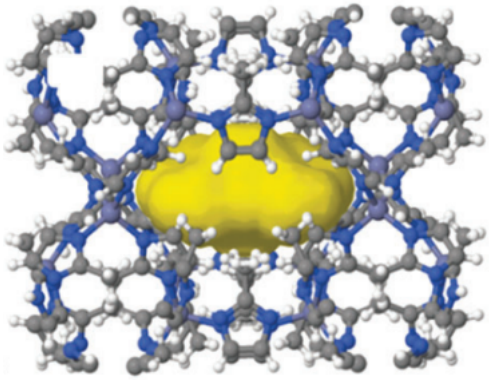

Figure 2.10: Chemical structure of ZIF-8L, by Chen et al. (2013).

One known issue with ZIF's (and MOF's) is their reported instability in contact with water, as described by both Zhang et al. (2014) and Zhang et al. (2015). For example, MOF-5 displayed serious corrosion after being exposed to humid conditions for two days, resulting in cracks and cavities in the particles. The cavities were found to increase in number and size over time. MOF's have a reported sensitivity to moisture, where particularly the ones with weak metal-ligand bonds are extra vulnerable. Several strategies have been tested and tried to increase the stability in contact with H_2O molecules, but most are coupled with some disadvantage. The issues arising might be a decrease in the particle porosity, tedious synthesis or complex instrumentation necessary.

Contrary to the ZIF nanoparticles, TiO_2 is an inorganic impermeable filler possessing advantageous hydrophilic properties. Impermeable fillers in a membrane can in some cases hinder the diffusion path, thus negatively affecting the permeability of penetrants. Vatanpour et al. (2012) reported fabricating membranes containing TiO_2 in a polyetersulfone-matrix. The results revealed that embedding polymers with the nanoparticle could greatly reduce fouling of the membrane. By reducing the chain mobility in polymers, TiO_2 could also be applied in reducing the aging phenomena commonly found in high free volume polymers (Ansaloni

and Deng, 2017).

The effect of diffusion pathways with permeable and impermeable fillers are given in Figure 2.11. The figure demonstrates how CO_2 might diffuse through the membrane compared to other species inhibiting less affinity for the nanoparticles. As the diffusion pathway is prolonged, the larger molecules will be affected to a larger extent, due to a lower affinity with the embedded molecules.The impermeable fillers in a MMM can interact with the polymer chains which can increase the free volume of the polymer and lead to better permeation properties (Bushell et al., 2013).

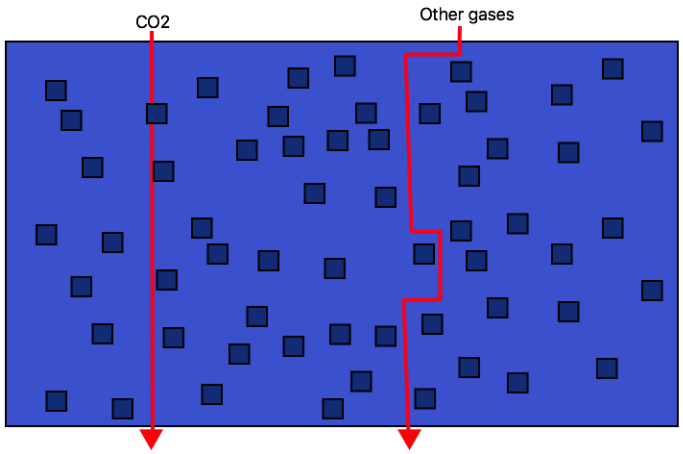

(a) Diffusion pathway with permeable nanofillers.

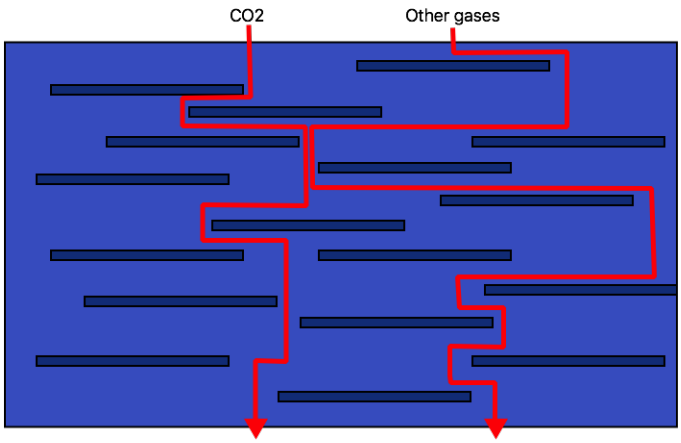

(b) Diffusion pathway with impermeable nanofillers.

Figure 2.11: Diffusion pathways in MMMs.

2.5 Effect of Humidity

In flue gas streams, the gas seldom consists of only the chosen species used for testing at lab-scale. Real gas streams will usually also include other minor compounds, e.g. water

molecules, H_2S and/or low molecular weight hydrocarbons. It is thus important to also investigate the effects of other compounds on the membrane, as a pin-point to how the membrane will react when scaled up to pilot plant or industrial size, where flue gas from secondary processes are used instead of pure gases from the lab. Water vapour can have varying effect based on water uptake and the hydrophilic properties of the membrane material. Materials that show more hydrophilic properties also have a higher affinity for H_2O-molecules. In many cases water vapour is found to change the properties of the membrane, by changing the permeability for one or several species. Swelling of the membrane and general changes in morphology have been observed in coherence with water uptake in the membrane, resulting in noteworthy transport property changes. In some cases, the selectivity of a membrane has been reversed. It is suggested by several professionals within the field that the water can form channels throughout the membrane matrix, creating liquid domains for which penetrants can be solubilized in and transported through the membrane (Ansaloni, 2014).

3 Method

The following sections give a description of materials and experimental methods used to prepare polymer membranes and the characterization of the membranes.

3.1 Materials

Membranes were made by using the high free volume polymer PTMSP supplied by Fluorochem. The polymer was mixed with different nanoparticles (ZIF-7, ZIF-8, ZIF-8L and TiO_2) to improve the properties of the membranes. The polymer and nanoparticles were solubilized in cyclohexane (C_6H_{12}) provided by Sigma-Aldrich. Some membranes were also prepared using chloroform ($CHCl_3$) from the same provider. ZIF-8 was provided in dry state by Sigma-Aldrich. ZIF-7 and ZIF-8L were synthesised by Dr. Zhongde Dai of the MEMFO Research Group (Department of Chemical Engineering, NTNU), following the procedure described by Zhong et al. (2015) and Li et al. (2013). TiO_2 was made at SINTEF Materials & Chemistry by Christelle Denonville for the use in the Doctoral Thesis by Seglem (2017). The TiO_2 particle size was 15 nm, which was aggregated with size >µm. The surface was treated with oleic acid to be stable in the wanted morphology while dissolved in toluene. Before use the particles were dried in a vacuum oven at 60°C overnight and the structure was determined using a scanning electron microscope (SEM). The gas used for permeation testing, a mixture of 90vol% N_2 and 10vol% CO_2 as well as pure CH_4, was provided by AGA.

3.2 Membrane Preparation

Dense self standing PTMSP membranes of approximately 50-100 µm were created in two different ways. In method (1) PTMSP was dissolved in cyclohexane at a concentration of 1wt% PTMSP in solvent and mixed with nanoparticles. The solution was sonicated for 4x45 minutes and cast into a Teflon Petri dish and left under a funnel for the solvent to evaporate. Method (2) consisted of creating two dope solutions as described by Zhang et al. (2012). Solution A contained a highly viscous solution of PTMSP in a small amount of solvent and solution B contained nanoparticles in solvent. Solution B was sonicated for 4-5 minutes using a Sonics Vibra-Cell^{TM} VC 70T, and then mixed into solution A. The mixture

of A and B was thereby sonicated once more for 4x45 minutes before the solution was cast onto a glass plate and cut using a casting-knife, illustrated in Figure 3.1, to obtain a suitable membrane thickness and uniform surface. The solution on the glass plate was covered by a glass container and left for the solvent to evaporate. If nothing else is stated the sonication was done using a VWR Ultrasonic Cleaner.

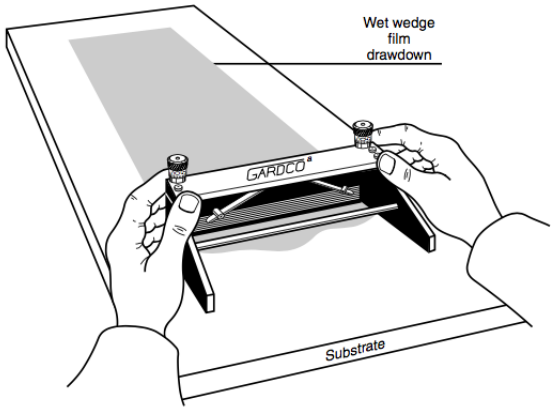

Figure 3.1: Casting-knife illustration, by Baker (2004d)

The concentration of nanoparticles in the membrane was determined by Equation (3.1).

$$wt\%NP = \frac{w_{NP}}{w_{NP} + w_{PTMSP}} \cdot 100 \tag{3.1}$$

where w is the weight in gram of nanoparticles (NP) and PTMSP respectively.

3.3 Membrane Characterization

The membranes were tested and characterized by the following methods. All membranes were dried in a vacuum-oven at 60°C overnight before any tests were performed.

3.3.1 Thermogravimetric Analysis - TGA

A TG F1 Libra by NETZSCH was used to perform a thermogravimetric analysis (TGA) of the membranes. The machine uses a thermobalance to detect changes in sample mass with

changing temperature and thereby gives information about the materials thermostability (Raade, 2009). The samples were analysed in the temperature-range 25-700°C at a constant heating rate of 10°C min^{-1}

3.3.2 Differential Scanning Calorimetry - DSC

For DSC-testing a DSC 214 Polyma by NETZSCH was used. In differential scanning calorimetry, a sample and a reference is investigated. The analysis method measures the difference in heat flow between the sample and reference while under a controlled temperature program (Flammersheim et al., 2003). The obtained data can give information on e.g. glass transition temperature and decomposition temperature of the material. In this case the temperature range was 25-300°C.

3.3.3 Fourier Transform Infrared Spectroscopy - FT-IR

FT-IR is short for Fourier Transform Infrared Spectroscopy, which is a method used to determine the chemical structures in molecules. During the procedure, infrared radiation is sent through a sample over a range of wavelengths, where the transmission/absorbance of radiation of the sample is measured. The wavelengths are in the range 650 - 4000 cm^{-1}, and the given spectra is an average of 16 scans. The given peaks in the spectrum will correspond to specific molecules so it will be possible to identify and quantify molecular species in a sample. The apparatus used for the FT-IR spectroscopy was Nicolet$^{\mathrm{TM}}$ iS$^{\mathrm{TM}}$ 50 FT-IR Spectrometer from Thermo Fisher (Bacsik et al., 2004; Bradley).

3.3.4 Scanning Electron Microscope - SEM

To investigate the morphology of the membranes, a TM3030Plus Tabletop Microscope from Hitachi was used to obtain images of the surface and cross-section of the samples. The microscope is a scanning electron microscope (SEM) where a focused electron beam is scanning the sample, while measuring back-scattering and secondary electrons. Cross-section samples of the membranes were prepared by freeze fracturing, where the membranes were submerged in liquid nitrogen and fractured to avoid squeezing the edges together or to create other dam-

ages that could affect the quality of the SEM images. Membranes for surface images was simply cut using a scalpel and mounted on the SEM-stub. The samples for SEM were coated with a thin gold layer to increase the sample conductivity, needed for the examination by SEM. Gold coating was performed using a Q150R Rotary-Pumped Sputter Coater/Carbon Coater from Quorum.

3.3.5 Mixed Gas Permeation

The permeability and separation factor of the different membranes were investigated by using a mixed gas permeation rig as seen in Figure 3.2, custom built by members of the MEMFO Group, Department of Chemical Engineering, NTNU. Mixed gas permeation testing was performed at room temperature with a feed pressure of 1.6 bar and a sweep pressure of 1.05 bar. Due to the partial pressure of CO_2 over the membrane, $\Delta p_{CO_2} \not\approx 0$, the membranes ability to separate different species is reported by using the separation factor α instead of the ideal selectivity α^{ID}. For the test a feed gas consisting of 90vol% N_2 and 10vol% CO_2 and pure CH_4 as sweep gas were used.

To obtain different values for relative humidity in the gas, both feed and sweep were split into two streams before contact with the membrane, where one went through several tanks filled with water and saturated, as depicted in Figure 3.2. The relative humidity was controlled by regulating the flow of dry and saturated gas in the feed and sweep gas.

Permeance, permeability and separation factor were calculated based on measurements from the rig. All calculations were performed using Excel-sheets provided by members of the MEMFO group. The measurements include average pressure and temperature, gas flow measured by a bubble flow meter and gas concentration in permeate and retentate measured by a gas chromatography (GC) connected to the setup. To obtain data for permeability, the membrane thickness was measured with a digital micrometer from Mitutoyo. Measurements were done 20 times per membrane, and an average thickness and standard deviation of the membranes were found based on these measurements. The membranes were cut out into circles of 2.4cm diameter to fit into the special built membrane cell.

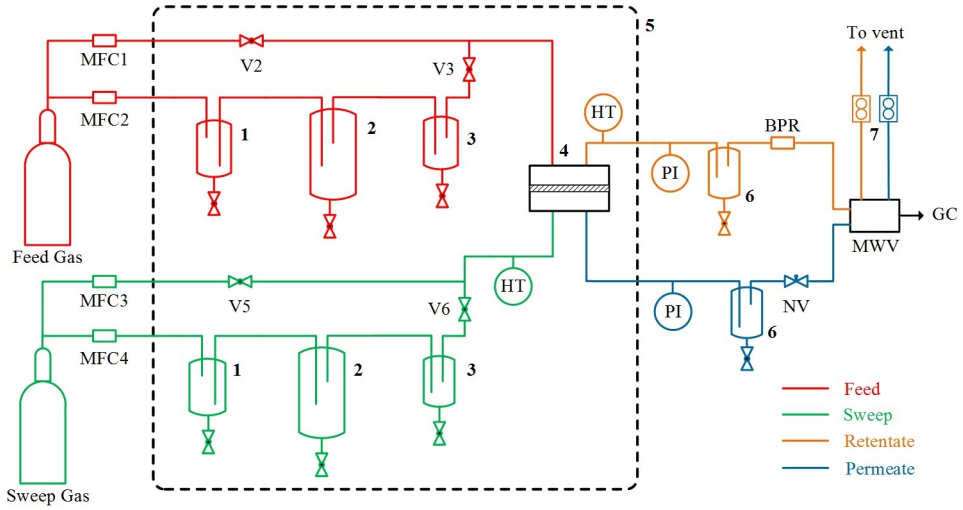

Figure 3.2: Flowsheet of Mixed Gas Permeation rig. The numbers/symbols on the figure is as follows; 1:Safety Trap, 2:Humidifier, 3:Droplets Trap, 4:Membrane module, 5:Heated Cabinet, 6:Water Knockout, MFC: Mass flow controller, NV:Needle valve, BPR:Back pressure regulator, PI:Pressure indicator, HT:Humidity and temperature sensor, MWV:Multi-way valve.

4 Results and Discussion

4.1 Membrane Preparation

The solvent chosen for making the membrane solution was based on literature findings. PTMSP is soluble in a wide range of solvents, which can have different effects on the permeability. Bi et al. (2000) and Bi et al. (2003) found that cyclohexane gave more permeable membranes, since the fractional free volume in the membrane was maximized compared to solvents such as toluene and tetrahydrofuran. In previous experimental work done in relation with the Specialization Project by Løining (2016), chloroform was used as solvent, as it was necessary to be able to solve both PTMSP and PEI (polyethyleneimine). Due to the carcinogenic properties of chloroform and that PEI is no longer used as an additive, it was decided to use a less harmful solvent. The effect of cyclohexane versus chloroform will be further discussed later on. Table 4.1 gives the thickness of every membrane, as well as the abbreviations for the different membranes that will be used throughout the rest of the thesis.

All data related to the pure PTMSP membrane made with chloroform, are collected during the Specialization Project in the fall of 2016, by Løining (2016).

Table 4.1: Abbreviations and thickness of membranes. The number in the parentheses are the weight-percentage of nanoparticles in the PTMSP polymer matrix based on Equation 3.1.

Polymer/Nanoparticle	**Abbreviation**	ℓ [µm]	STD [µm]
PTMSP	PTMSP	63.4	2.1
PTMSP/ZIF-7	ZIF-7(30) [1]	51.5	15.4
PTMSP/ZIF-8	ZIF-8(20)	63.4	4.9
PTMSP/ZIF-8L	ZIF-8L(20)	94.0	2.1
PTMSP/ZIF-8L	ZIF-8L(10)	57.1	0.8
PTMSP/ZIF-8L	ZIF-8L(5)	62.9	4.0
PTMSP/TiO_2	TiO_2(25)	49.4	1.0
PTMSP/TiO_2	TiO_2(5)	55.4	1.4

Li et al. (2013) found that a loading of 34wt% ZIF-7 was too high, while membranes containing 22wt% ZIF-7 showed increased properties. The ZIF-7(30) membrane was prepared

[1]The ZIF-7(30) membrane was made using chloroform, as this membrane was cast in a Petri dish, and a solvent with a more rapid evaporation was required.

prior to reading this article, and thus the following weight-percentage of the membranes were reduced. When preparing the membranes containing TiO_2, there were minor inaccuracies in measurement of polymer and nanoparticles, and thus 25wt% and 5wt% membranes were prepared instead of 20wt% and 10wt%.

The membrane preparation ended up being quite challenging. Previously, self standing PTMSP/PEI blend membranes had been fabricated by pouring the polymer solution into Teflon Petri dishes and left to evaporate under controlled conditions. Cyclohexane has a boiling point 20°C higher than chloroform, and the evaporation took an extended amount of time. When the solvent finally evaporated, the polymer-nanoparticle dispersion had separated, and the nanoparticles had formed a layer on the bottom of the prepared membrane (which is depicted in Figure 4.11 later on). Subsequently, membranes were fabricated by pouring a highly viscous solution onto a glass plate and spreading it out with a casting-knife. For this method, the challenge was to increase the evaporation time. When the solvent evaporated too fast the membrane contracted, destroying the homogeneous surface. By placing a glass container upside down over the glass plate with the membrane, the evaporation time was slowed down to the extent that a membrane with a smooth surface was successfully fabricated. Some illustrative images of fabricated membranes can be found in Appendix A.

Effort was also made to fabricate and test membranes of PI, specifically 6FDA-Durene, and ZIF-8L. Several membranes of pure PI and PI/ZIF-8L (2wt%, 4wt% & 10wt%) were prepared using method (2), with the dope solutions and casting knife. From the images taken in SEM it was clear that all membranes contained a huge amount of tiny holes at the surface, and bubbles in the membranes were also visible with the naked eye. For several mixed gas permeation tests the permeability found for the membranes was extremely high. As reported by Lin and Chung (2001), the CO_2 permeability was found to be less than 700 Barrer and a selectiviy of 20. In the gas permeation test the permeability was tens of thousands of Barrer, with a selectivity below 3. The poor permeability and selectivity results, the permeation test was not at all in accordance with literature. Since PTMSP is the main focus of the current thesis, further testing of the MMM utilizing PI was terminated. Parts of the data collected for the PI/ZIF-8L membranes can be found in Appendix B.

4.2 Membrane Characterization

In the following sections the characterization of the membranes will be discussed.

4.2.1 Thermal Properties

Thermal stability of membranes is a property which is highly valued in membrane separation. By conducting a Thermogravimetric Analysis the stability can be investigated. The results for the thermal analysis are given in figures 4.1-4.4.

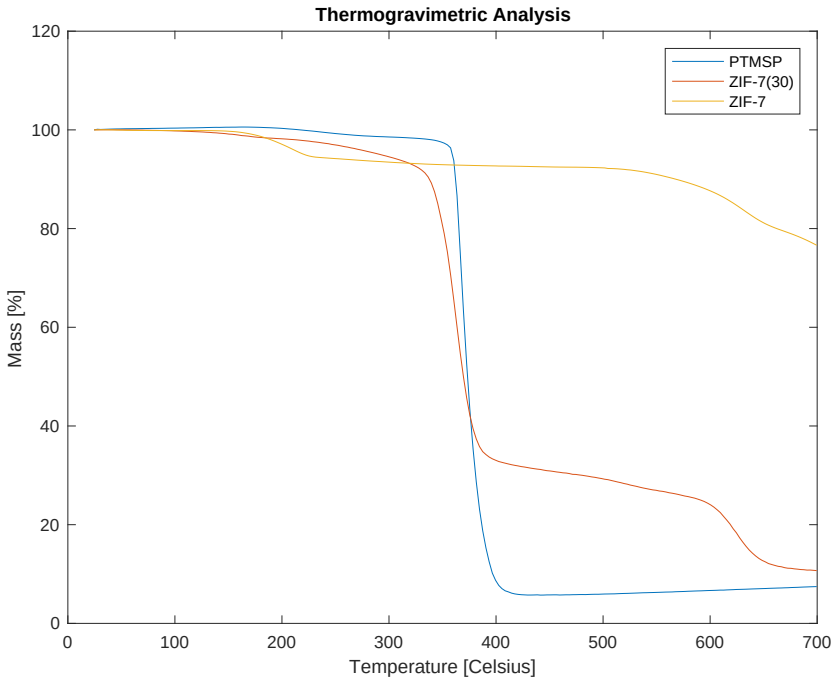

Figure 4.1: Thermogravimetric Analysis of PTMSP/ZIF-7 membranes.

From Figure 4.1 it is observed that ZIF-7 has a high thermal stability, with a weight-loss of only 23wt% up to 700°C. T_{onset} for the degradation for ZIF-7 starts already at 177°C compared to T_{onset} for PTMSP at 360°C. PTMSP is stable up to a higher temperature, but the degradation is more severe in the entire temperature range. It is clear that adding ZIF-7 is increasing the thermal stability of the hybrid PTMSP/ZIF-7 membrane.

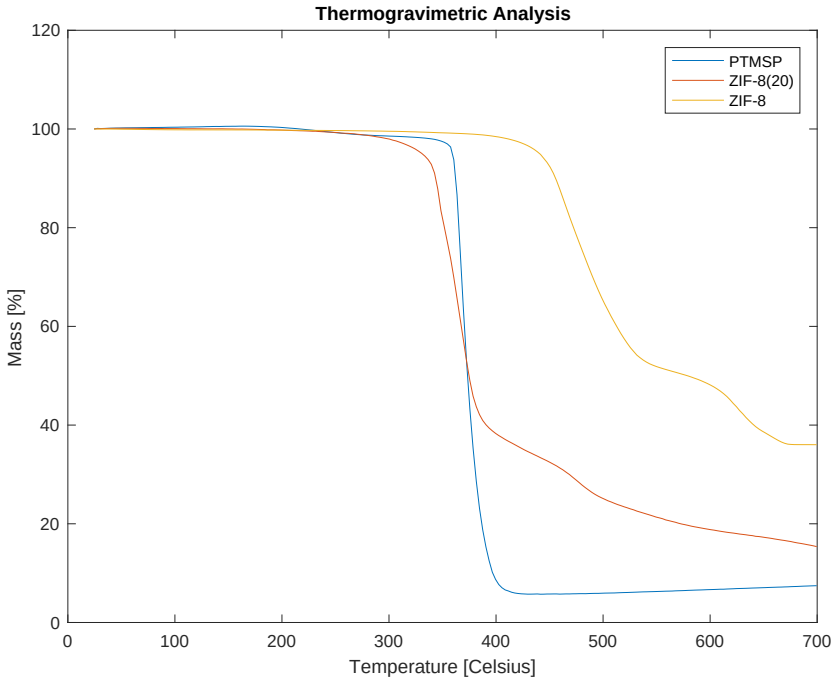

Figure 4.2: Thermogravimetric Analysis of PTMSP/ZIF-8 membranes.

In Figure 4.2 ZIF-8 display a lower thermal stability than the ZIF-7 nanoparticles. At 700°C, ZIF-8 have experienced a 66% weight-loss, where the decomposition starts to happen around 439°C. Still, the thermal stability is better for ZIF-8 than for pure PTMSP, and the membranes become more stable by adding ZIF-8 into the polymer matrix. T_{onset} for ZIF-8(20) is found to be 339°C, which is lower than both pure PTMSP and pure ZIF-8. The degradation also occurs at a lower temperature, but ends up having a mass weight-loss between the two pure compounds. The early start of degradation might be attributed to some small error in the experimental test such as presence of a contaminant, e.g. solvents or water vapour.

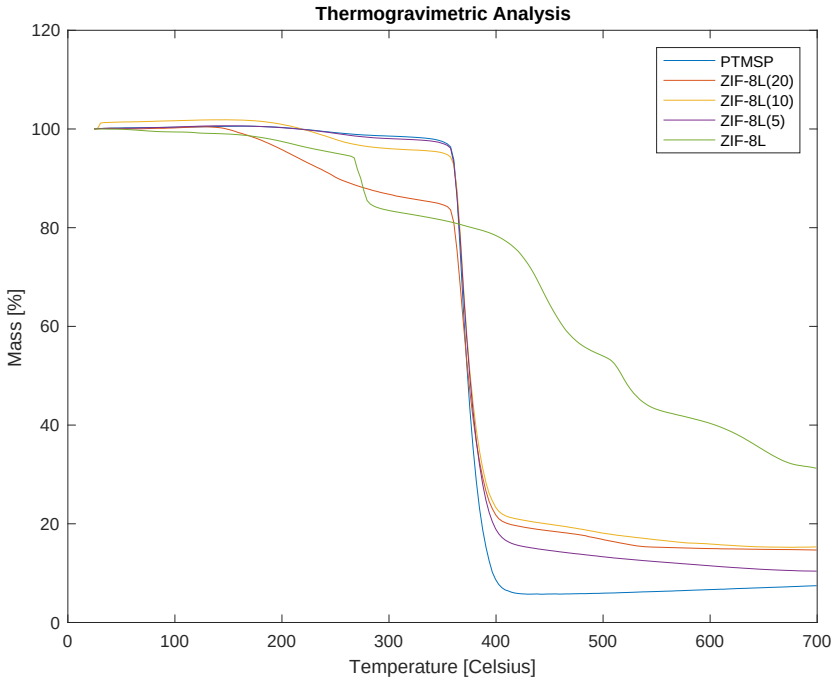

Figure 4.3: Thermogravimetric Analysis of PTMSP/ZIF-8L membranes.

Of all the nanoparticles, ZIF-8L are the one with lowest thermal stability, given by Figure 4.3. T_{onset} for degradation is at 268°C, and after being exposed to 700°C, only 31wt% of the nanoparticle remains. ZIF-8L(20) exhibit a curious degradation, not following the main trend, which might be due to some impurities in the sample. For the ZIF-8L membranes in general, as for the ZIF-8 membranes, the terminal weight of the membranes are in coherence with the amount of additives in the membrane matrix.

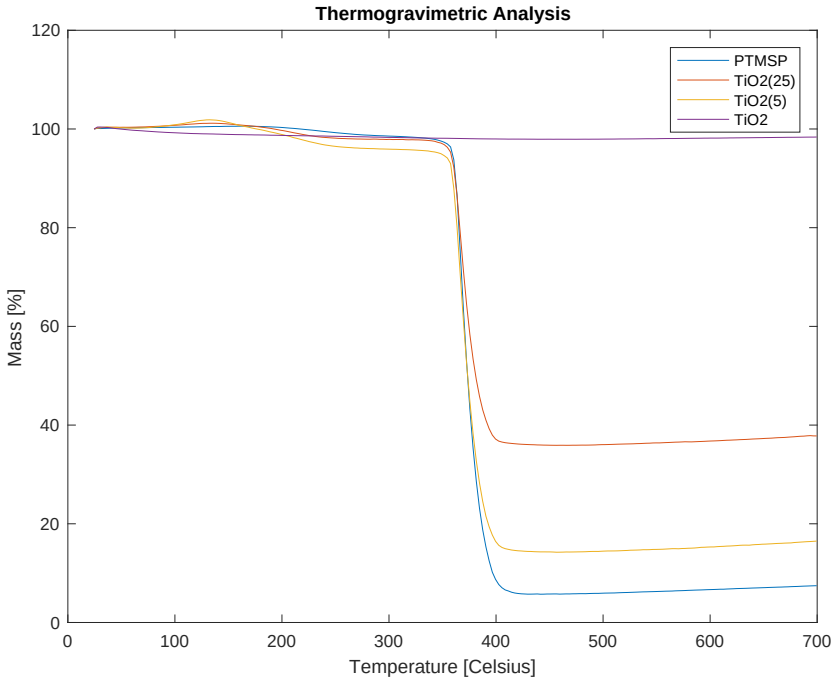

Figure 4.4: Thermogravimetric Analysis of PTMSP/TiO_2 membranes.

Figure 4.4 gives the thermal stability of the PTMSP/TiO_2 membranes and pure TiO_2 particles. The weight-loss of TiO_2 is less than 2wt% of original weight, leading to the conclusion that TiO_2 is extremely thermally stable in the given temperature range. This property can be observed in the MMMs of PTMSP/TiO_2 as well, where the trend exhibit increased thermal stability with increased amount of filler in the membranes.

To sum up, adding more thermally stable nanoparticles into the PTMSP matrix, will in all cases increase the final thermal stability of the membranes. This property can be especially important for separating CO_2 from flue gas. The fact that the membrane can be stable at higher temperatures, makes it avoidable to spend energy/money on reducing the temperature of a waste-stream.

Consolati et al. (1996) report the T_g of PTMSP to be higher than the decomposition temperature around 379°C. This is closely resembling the results of the thermal analysis done on PTMSP in this work, with start of decomposition around 360°C. A rapid decomposition occur with a subsequent weight-change of over 90wt%. Normally when running a DSC, the temperature is taken in a "loop" to first remove any residual humidity/solvents in the

sample, before cooling and reheating. In the case of PTMSP this will work against its intention, because the sample will start to decompose already in the first heating-run, and thus destroying the sample. If the DSC was done in a range over the T_g of a polymer, a sharp increase in the heat flow would be visible. As nothing out of the ordinary are given by the DSC data, the figures can be found in Appendix C.

4.2.2 Structural Properties

The following graphs display the results of the FT-IR spectra for all membranes and materials.

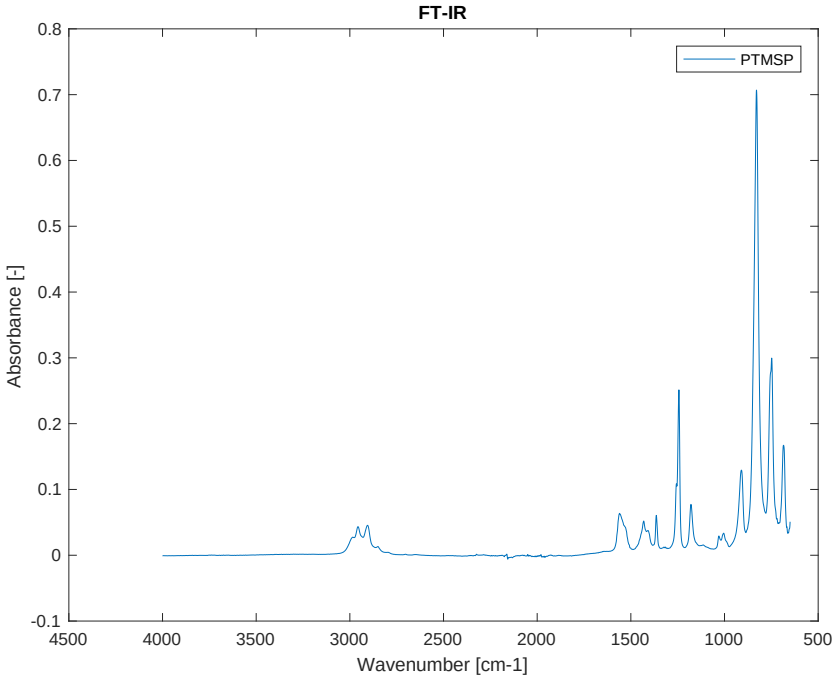

Figure 4.5: FT-IR of pure PTMSP.

Figure 4.5 depict the FT-IR of a pure PTMSP membrane, showing the absorbance of light at different wavelengths. The results are in coherence with an IR spectra of PTMSP given by Nagai et al. (2001). The first peak at 1540 cm^{-1}, are contributed to the stretching of the double bond C═C. The larger peak at 1240 cm^{-1} is due to deformation of the SiC—H bond, while the greatest peak at 820 cm^{-1} is due to stretching of the C—Si bond. The FT-IR spectra is in accordance with other results by Nagai et al. (2001), and the specific peaks match with the given chemical structure, given by Figure 2.5

The peak present around 3000 cm^{-1} for PTMSP in Figure 4.5 is also present in all the mixed matrix membranes, but not existing for the four nanoparticles. Thus, the following figures only present a segment of the FT-IR spectra where there are several visible changes between membranes and nanoparticles. The full spectra for all the membranes/nanoparticles can be found in Appendix D.

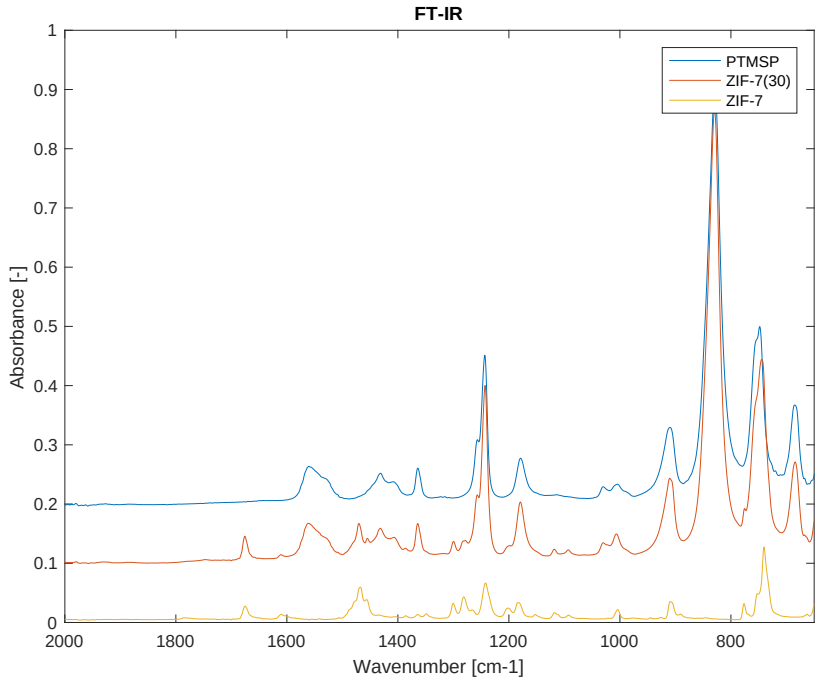

Figure 4.6: FT-IR of PTMSP/ZIF-7 membranes and ZIF-7 nanoparticles.

The FT-IR spectrum of ZIF-7 given by Figure 4.6 exhibit several peaks in the range 650-2000 cm^{-1}, and are in accordance with the results given by Kang et al. (2013). Here, especially the peaks at 1455 cm^{-1} and 777 cm^{-1} are of interest. They are identified as the peaks for the C═C and C—H, respectively. These bonds are from the functional group of benzene in benzimidazole found in ZIF-7. In ZIF-7(30), the peak at 1455 cm^{-1} are clearly present, while at 777 cm^{-1} the peak is barely detectable. Still, the results lead to the conclusion that the PTMSP/ZIF-7 MMM was successfully fabricated.

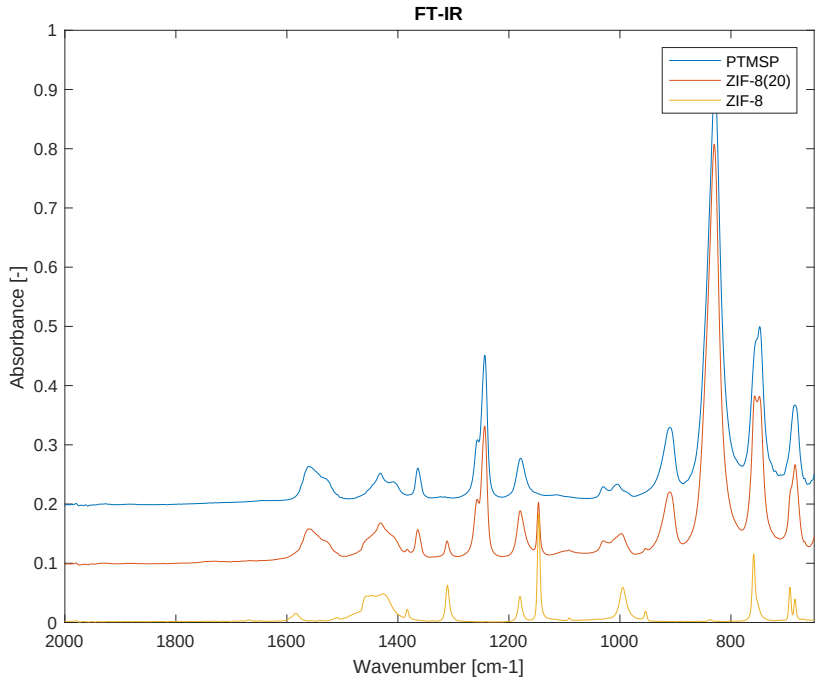

Figure 4.7: FT-IR of PTMSP/ZIF-8 membranes and ZIF-8 nanoparticles.

Hu et al. (2011) have investigated the IR of ZIF-8, and determining the sources for the different peaks. At 1584 cm^{-1} a peak is found, related to the stretching of C—N bond found in the 2-methylimidazole ring in ZIF-8, as presented in Figure 4.7. The group of peaks in the range 1350-1500 cm^{-1} are linked to the ring stretching. In the range 900-1350 cm^{-1} the peaks are coupled with in-plane ring bending, while the peaks present below 800 cm^{-1} are caused by out-of-plane bending. Most peaks coincide with the spectrum for PTMSP, but some are only present for ZIF-8 and ZIF-8(20). Particularly a peak at 1146 cm^{-1} and 1310 cm^{-1} corresponding to C—H vibrations are only found in the two latter. Again, the results support the successful fabrication of the PTMSP/ZIF-8 MMM.

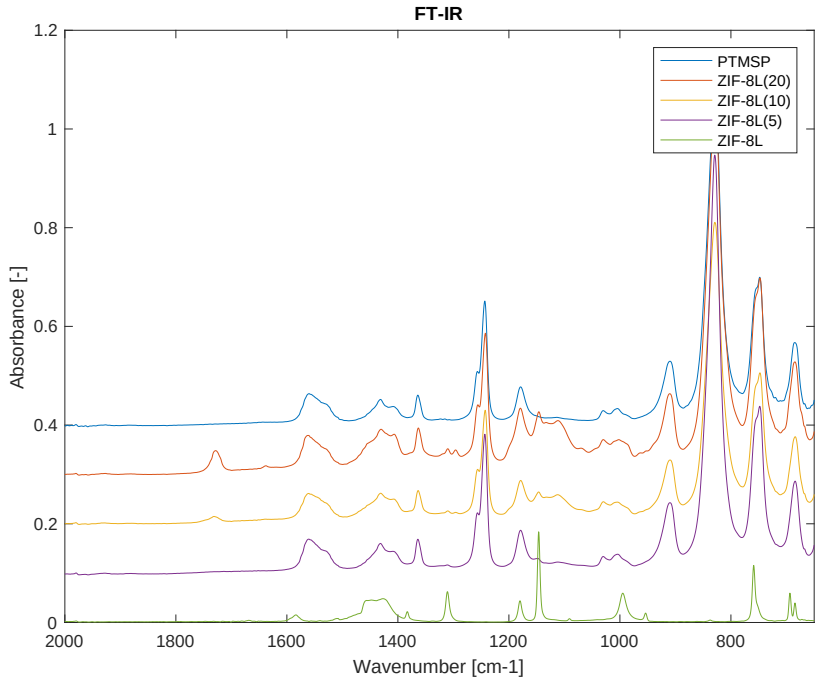

Figure 4.8: FT-IR of PTMSP/ZIF-8L membranes and ZIF-8L nanoparticles.

The FT-IR of ZIF-8 in Figure 4.7 and ZIF-8L in Figure 4.8 are identical since the chemical structure is exactly the same, and the different morphology do not affect the results. Thus, the same peaks are present in both figures. Unique for Figure 4.8 is how the intensity of the peaks in the MMMs due to ZIF-8L are increasing with increasing concentration of nanoparticles. The results are in accordance with what is reported by Liu et al. (2014).

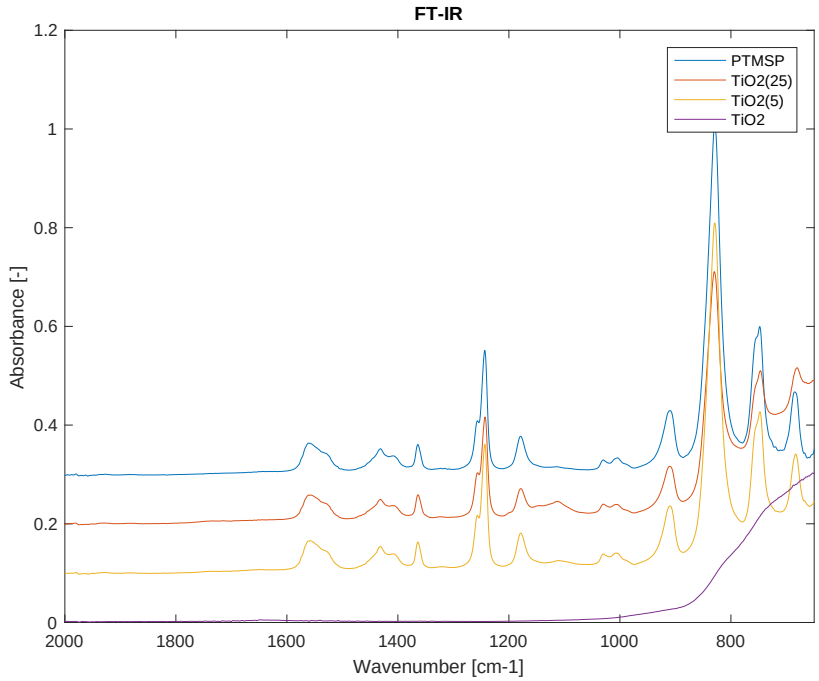

Figure 4.9: FT-IR of PTMSP/TiO_2 membranes and TiO_2 nanoparticles.

The TiO_2-particles have a rather non-distinct IR-spectrum, being approximately a flat line, until it gradually increases as it comes closer to 1000 cm^{-1}. Murashkevich et al. (2008) reports that the very broad peak will reach its maximum around 526 cm^{-1}, and that there should be a "shoulder" around 768 cm^{-1} due to symmetric stretching vibrations in the $Ti-O$ bond. From Figure 4.9 it is observed that the TiO_2drop membranes exhibit the same behaviour as pure PTMSP, but that they towards 650 cm^{-1} have an increase in the intensity of the peaks, in accordance with the concentration of TiO_2 in the membranes.

4.2.3 Morphology

Cross-section images

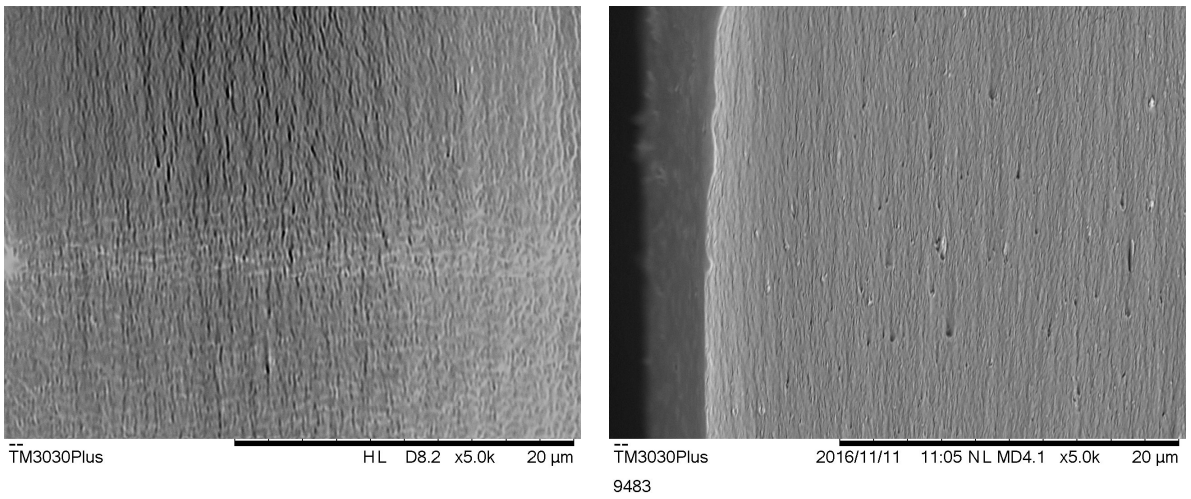

(a) PTMSP made with cyclohexane. **(b)** PTMSP made with chloroform,

Figure 4.10: Cross-section images of a pure PTMSP membrane.

As mentioned in Section 4.1, the solvent used to fabricate pure PTMSP membranes can affect the morphology. This is evident when comparing the cross-section of the PTMSP made with cyclohexane and chloroform in Figure 4.10. The cross-section of the membrane is still uniform when using cyclohexane, but the structure is slightly different, looking more cracked.

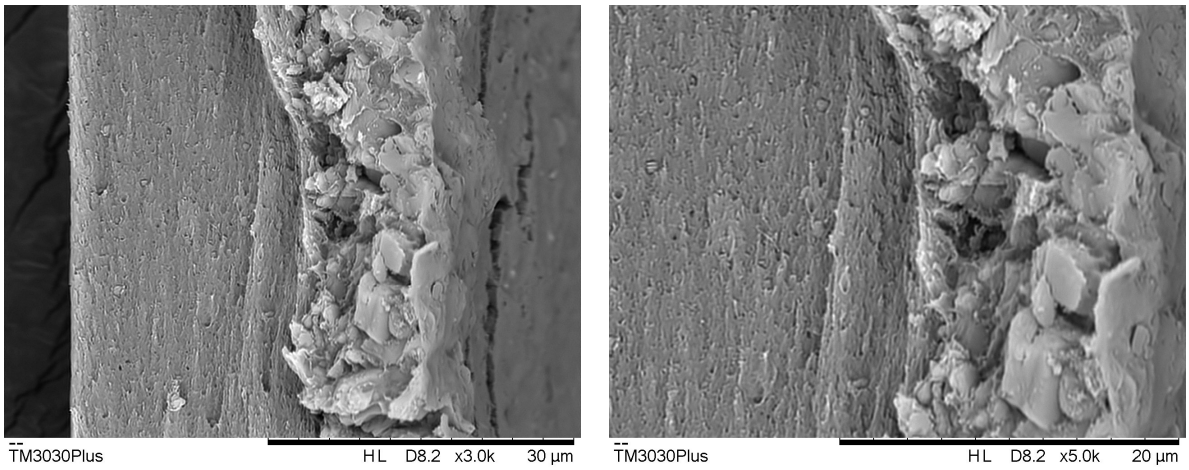

(a) Magnification: 3.0k **(b)** Magnification: 5.0k

Figure 4.11: Cross-section images of ZIF-7(30), made with chloroform.

Figure 4.11 display the cross-section SEM images for the ZIF-7(30) membrane. This membrane was cast in a Petri dish where the solvent ($CHCl_3$) slowly evaporated, and the only one of its kind that was tested further. From the images it is clear that the evaporation time affected the final product to a great extent, as all the ZIF-7 have fallen to the bottom due to gravity, forming a thick layer of nanoparticles at the bottom, as is visible on the left side in the images. It is assumed that the rest of the membrane interface consists of mostly PTMSP, but still it does not look quite as uniform as the pure PTMSP in Figure 4.10

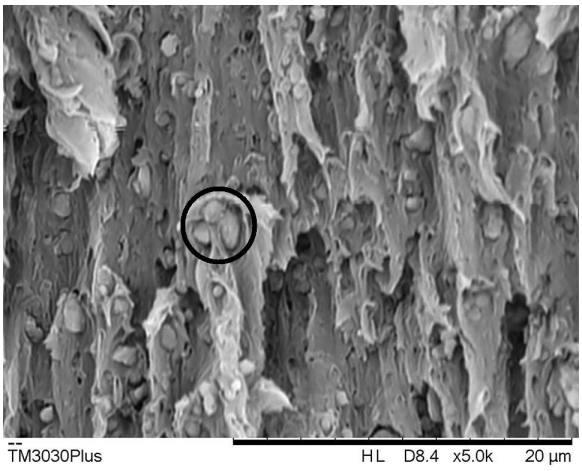

Figure 4.12: Cross-section image of ZIF-8(20).

In the ZIF-8(20) membrane, there is mostly an even distribution of particles visible through the MMM, although some agglomeration is visible, as given by the highlighted area in Figure 4.12. The nanoparticles are clearly visible within the membrane matrix, but it is obvious that the addition of ZIF-8 greatly change the morphology in comparison with the pure polymer membrane. Some holes are observed in the cross-section, which can be due to a number of reasons. Two probable explanations could be either that the holes are caused by damage when creating the cross-section sample of the membrane, or that it is voids caused by poor adhesion between polymer and nanoparticle.

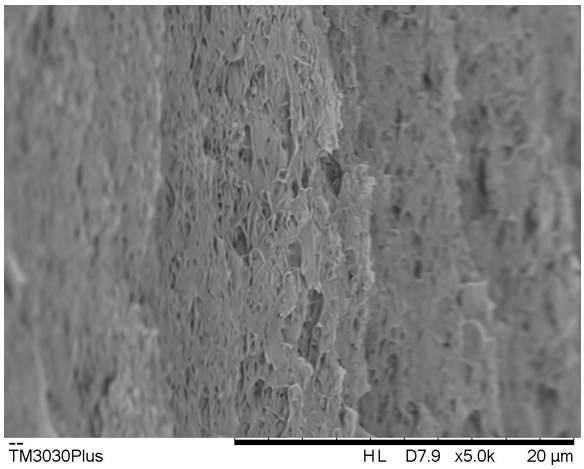

(a) ZIF-8L(20).

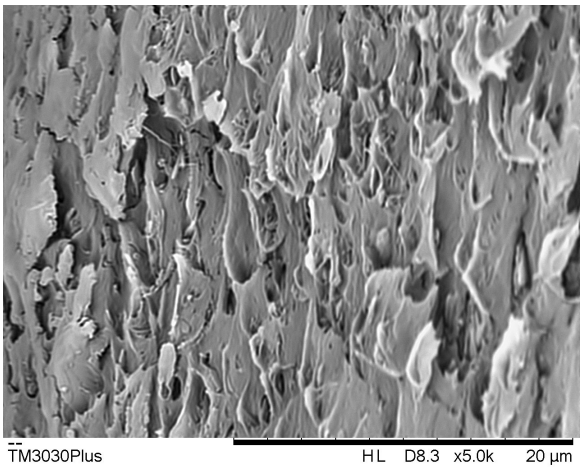

(b) ZIF-8L(10).

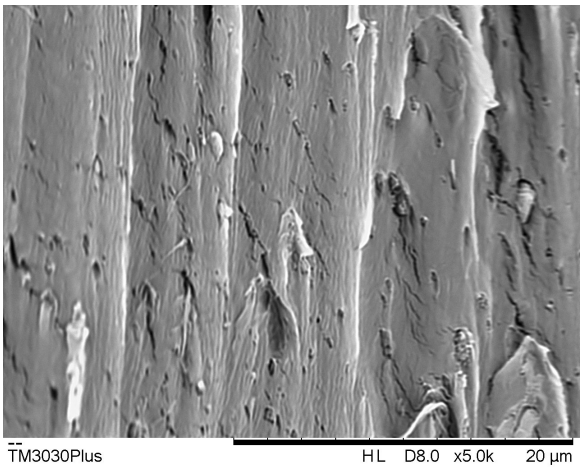

(c) ZIF-8L(5).

Figure 4.13: Cross-section images of ZIF-8L membranes.

Figure 4.13 display the cross-section of the ZIF-8L membranes. In ZIF-8L(20) the structure is visibly different from all the previous membranes presented. The two-dimensional ZIF-8L are having a different effect on the pattern present within the membrane. The difference in ZIF-8L concentration in the membrane are shown to have a relatively large effect, as there is a clear change in the morphology in the three membranes with varying concentration of ZIF-8L. Evident from the figure is that only 5wt% of nanoparticles have a relatively small effect on the morphology, and the membrane is somewhat resembling the pure PTMSP membrane. In the membrane containing 20wt% a clear pattern is emerging in the membrane, and to some extent it can also be found in the membrane containing 10wt% ZIF-8L.

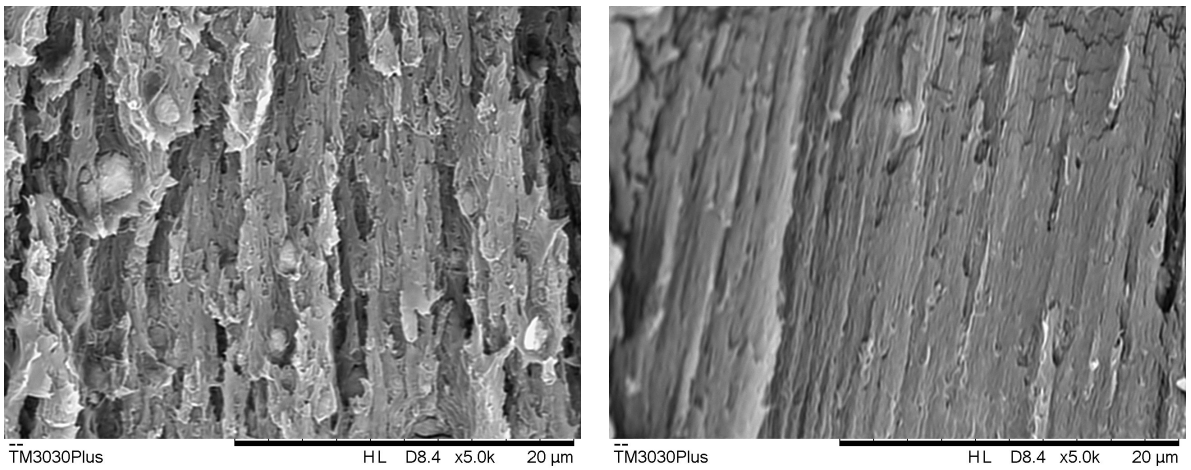

(a) $TiO_2(25)$. **(b)** $TiO_2(5)$.

Figure 4.14: Cross-section images of TiO_2 membranes.

25wt% TiO_2 make a great impact on the membrane morphology, as observed in Figure 4.14. The TiO_2 particles with a particle size of approximately 2 µm is clearly visible throughout the membrane, and the membrane morphology is closely resembling the one found for ZIF-8(20) in Figure 4.12. In $TiO_2(5)$ the small amount of nanoparticles makes the morphology similar to the pure PTMSP membrane and ZIF-8L(5). An altering of morphology compared to pure PTMSP is still observed, where the membrane reveal a flaky look, as if a large number of very fine layers were put on top of each other.

Surface images

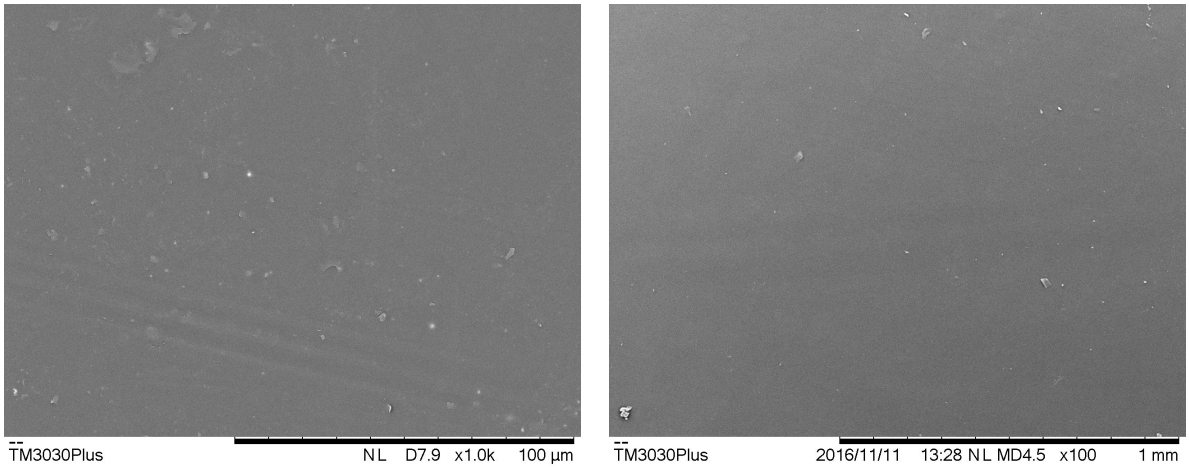

(a) PTMSP made with cyclohexane. **(b)** PTMSP made with chloroform.

Figure 4.15: Surface images of pure PTMSP membranes.

The images of pure PTMSP membranes made with cyclohexane and chloroform are given in Figure 4.15. The surface morphology for the pure polymer membranes are quite homogeneous, with small particles which is believed to be dust/particles from the surrounding environment. There is no significant difference in surface morphology of the two membranes, even though a difference is observed in the cross-section. This seem reasonable since the solvent is reported to have an effect on the free volume of the membranes.

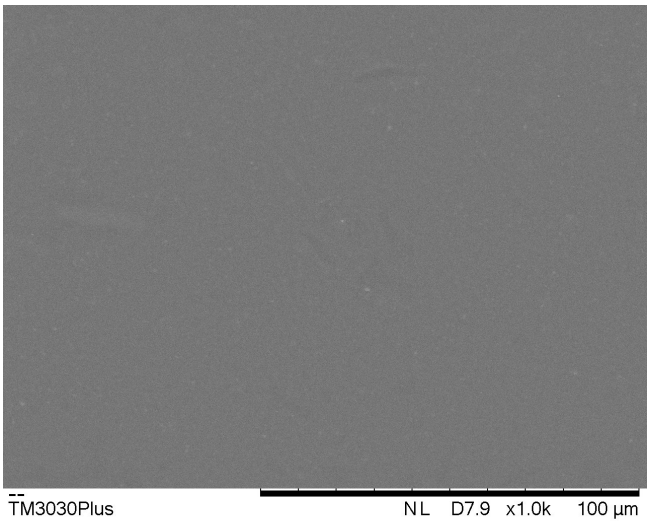

Figure 4.16: SEM surface image of ZIF-7(30).

Figure 4.16 depicts the surface SEM image of the ZIF-7(30) membrane. Even with a relatively high additive-content compared to the others, there is no visible nanoparticles at the surface. It is reasonable to believe that this is the "top side" of the membrane, seen in relations with the cross-section (Figure 4.11) which strengthens the assumption that nearly all nanoparticles are found at the bottom of the membrane, due to sedimentation.

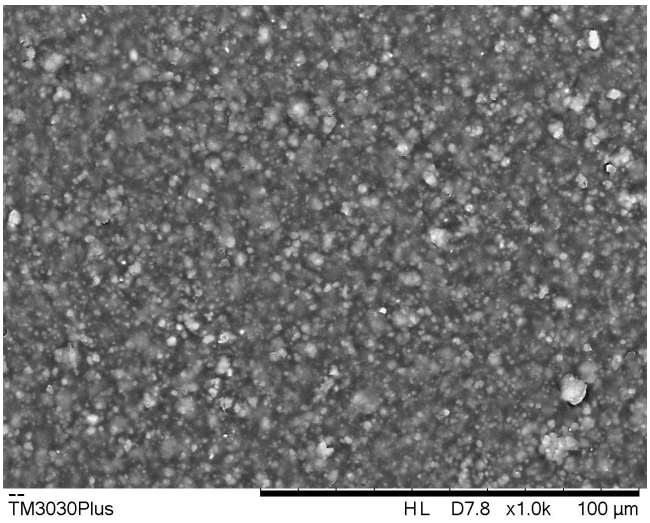

Figure 4.17: SEM surface image of ZIF-8(20).

Different from ZIF-7(30), the nanoparticles are clearly visible at the surface of ZIF-8(20), as displayed in Figure 4.17. Combined with the images of the cross-section, it can be concluded that the method of membrane fabrication can give a MMM with a good dispersion of ZIF-8 in PTMSP, but that there might be some problems concerning the interface between polymer and ZIF-8.

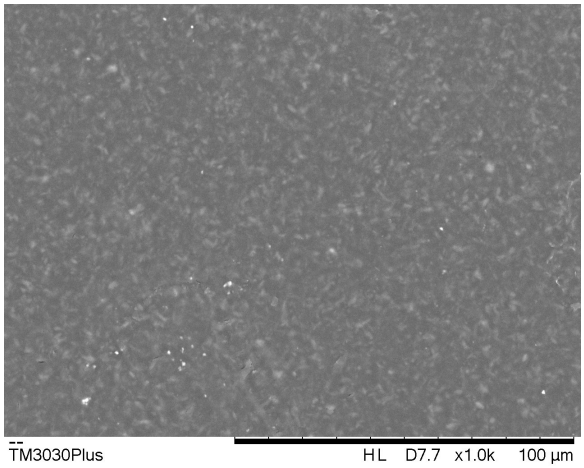

(a) ZIF-8L(20)

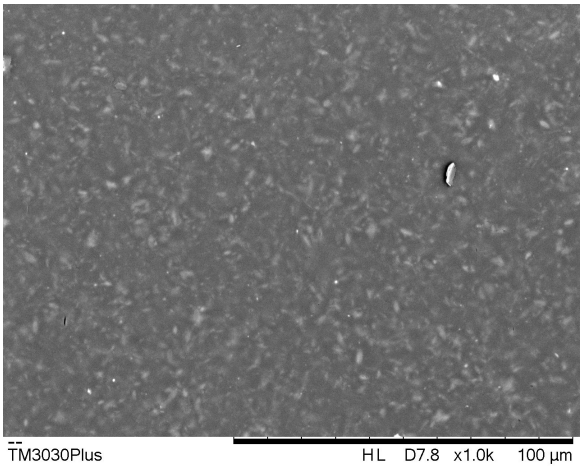

(b) ZIF-8L(10)

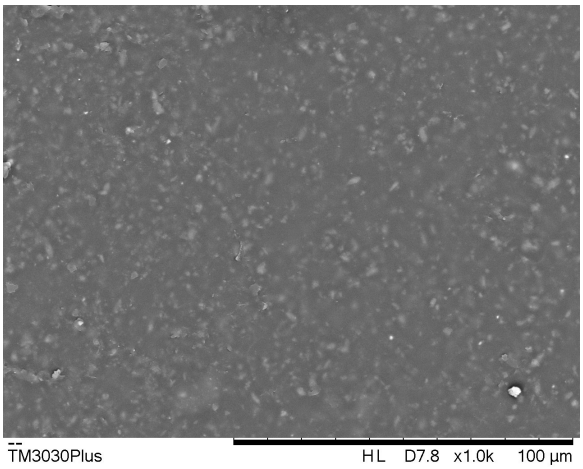

(c) ZIF-8L(5)

Figure 4.18: Surface images of ZIF-8L membranes.

The leaf-like structure of ZIF-8L can be observed just at the surface interface in the membranes containing this nanoparticle, as presented in Figure 4.18. No large deviations are

found between the different concentrations, and overall, the surface images show signs that nanoparticles are evenly dispersed throughout the polymer matrix, with no obvious agglomeration.

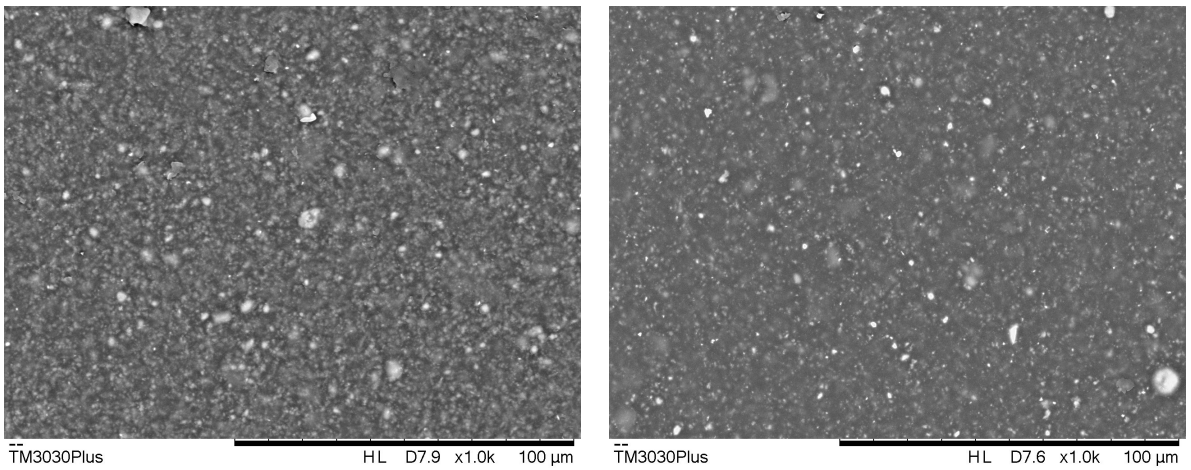

(a) $TiO_2(25)$. **(b)** $TiO_2(5)$.

Figure 4.19: Surface images of TiO_2 membranes.

Figure 4.19 present the surface images for the $TiO_2(25)$ and $TiO_2(5)$ membranes. Here the surface differentiates a great deal from the pure PTMSP membrane, with what appears to be a quite rough surface morphology. The visible amount of nanoparticles decrease with a descending additive concentration in the membranes.

4.2.4 Mixed Gas Permeation

In the following section the recorded data from the mixed gas permeation tests are reported. A summary of the permeation data for all membranes at dry conditions, 0% relative humidity (RH), as well as N_2 permeability can be found in Appendix E. The Robeson Upper Bound is given in Figure 4.20, along with a summary of all the membranes tested during this work. The figure display the CO_2 permeability plotted against the separation factor α_{CO_2,N_2} at dry conditions (0% RH). From the figure it is clear that none of the membranes are close to reaching the Upper Bound, thus resulting in membranes with unexceptional performance related to both CO_2 permeability and separation factor α. Except for the ZIF-8L(20), the membranes exhibited a permeability increase of 18-58%, and a decrease in separation factor of 2-34% compared to a pure membrane. The results will be further discussed in relation to each additive in the polymer matrix.

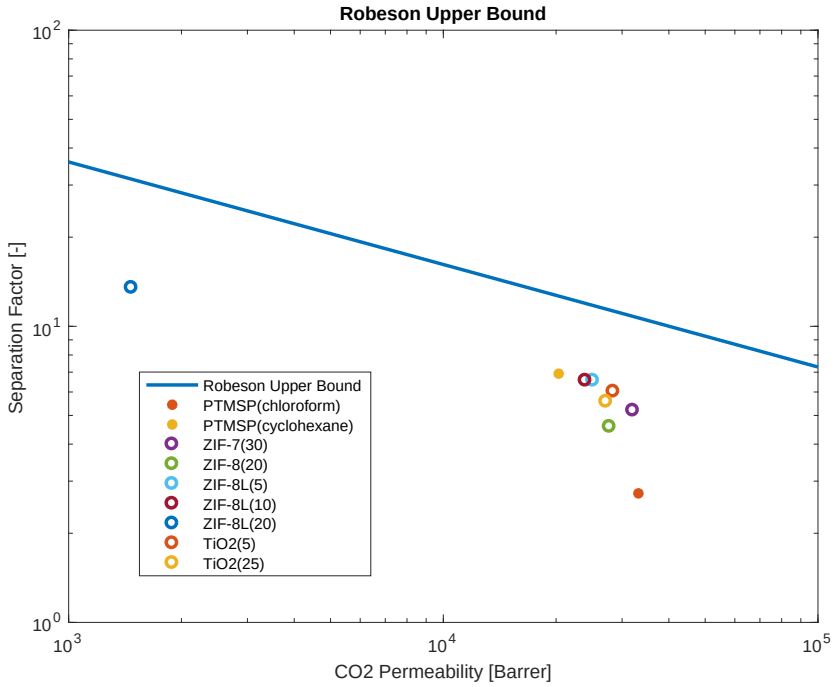

Figure 4.20: Robeson Upper Bound Plot.

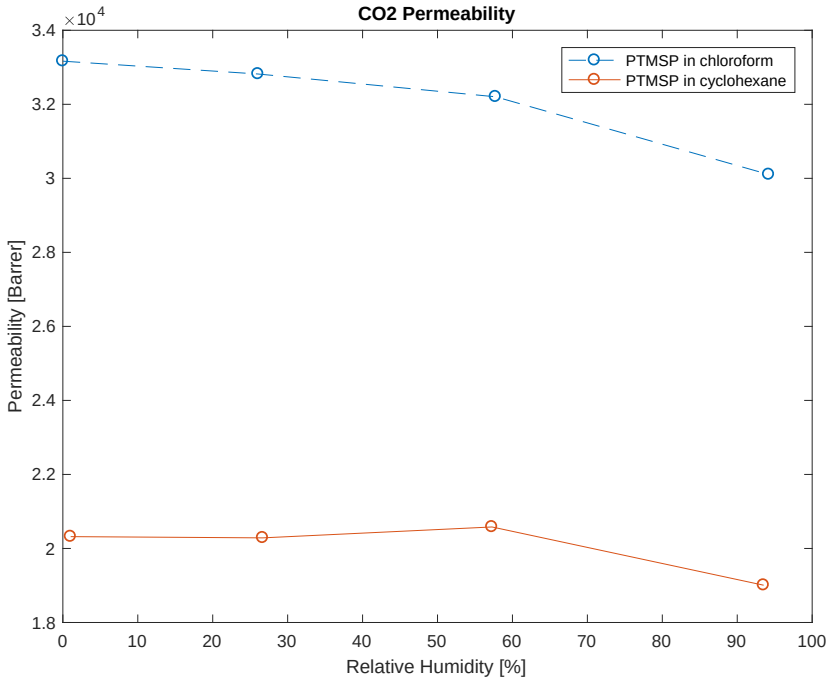

Figure 4.21: CO_2 permeability in pure PTMSP membranes.

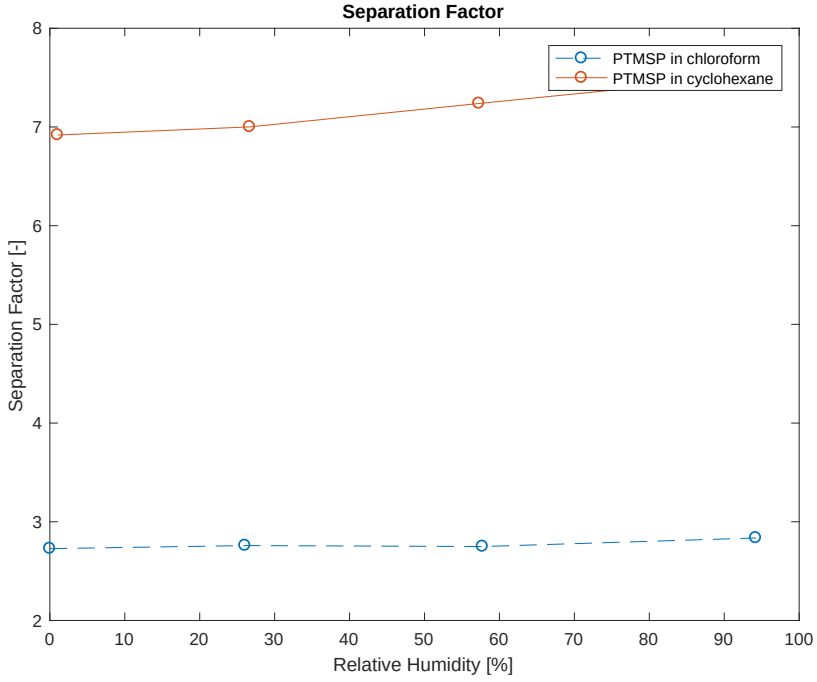

Figure 4.22: Separation factor in pure PTMSP membranes.

As discussed in Section 4.1, the solvent used to fabricate PTMSP membranes can greatly affect the membrane properties, as presented in Figure 4.21. Since the high permeability of PTMSP is credited to the high amount of free volume in the polymer, it can be assumed that using cyclohexane instead of chloroform reduces the free volume in the membrane. From Figure 4.22, showing α, it is clear that the N_2 permeability is reduced to a greater extent than for CO_2. Even though the permeability of CO_2 is reduced from nearly 33000 Barrer, a permeability of 20000 Barrer is still very good in relation to gas separation. A positive side-effect to the decreased permeability is the increased separation factor of the membrane, going from below 3 to 7. If the pure PTMSP membranes are compared to each other in the Robeson Plot given by Figure 4.20, it is clear that cyclohexane as a solvent bring the separation properties of the membrane closer to the Robeson Upper Bound.

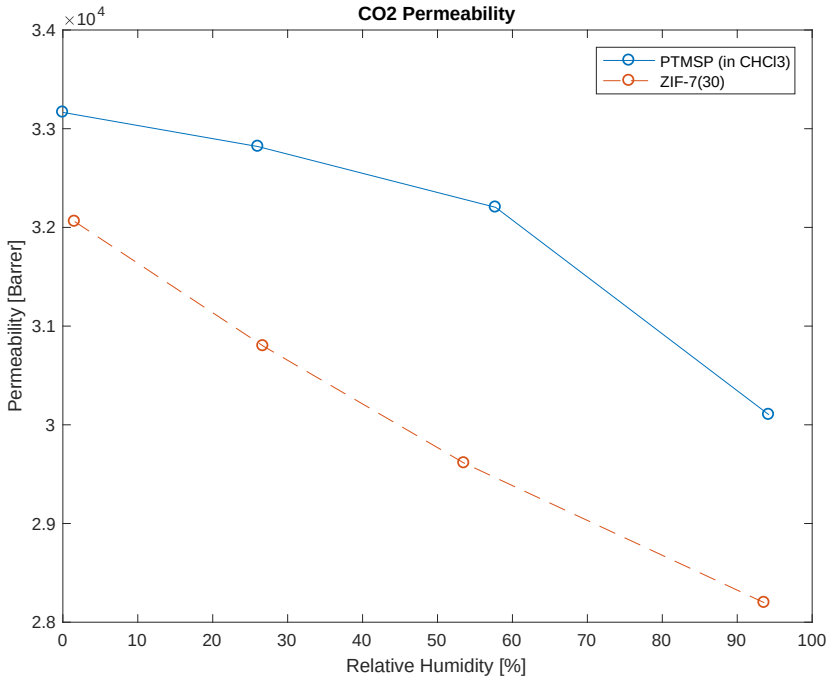

Figure 4.23: CO_2 permeability in PTMSP/ZIF-7 membranes.

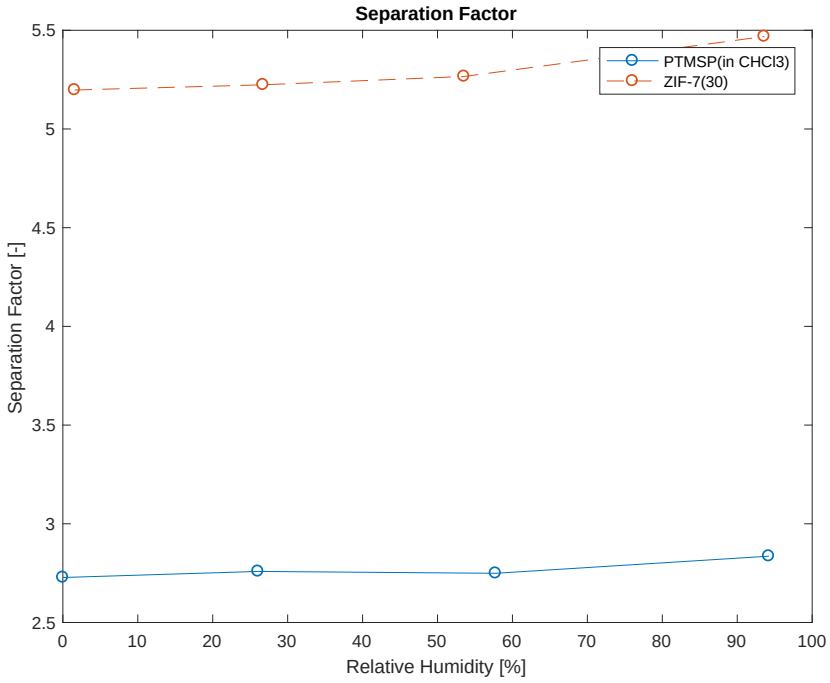

Figure 4.24: Separation factor in PTMSP/ZIF-7 membranes.

Since the ZIF-7(30) membrane was created using chloroform, it will thus be compared to the permeability data of the PTMSP membrane fabricated using chloroform. Figure 4.23 report the CO_2 permeability of the MMM compared to the pure PTMSP membrane. At dry conditions the permeability of ZIF-7(30) is reduced by only 3% compared to the pure membrane, while there is a considerable increase in the separation factor, thus the permeability of N_2 have been affected to a greater extent. Since there is no substantial change in the CO_2 permeability, it is believed that the membrane was fabricated without big voids forming at the interface between polymer and nanoparticle.

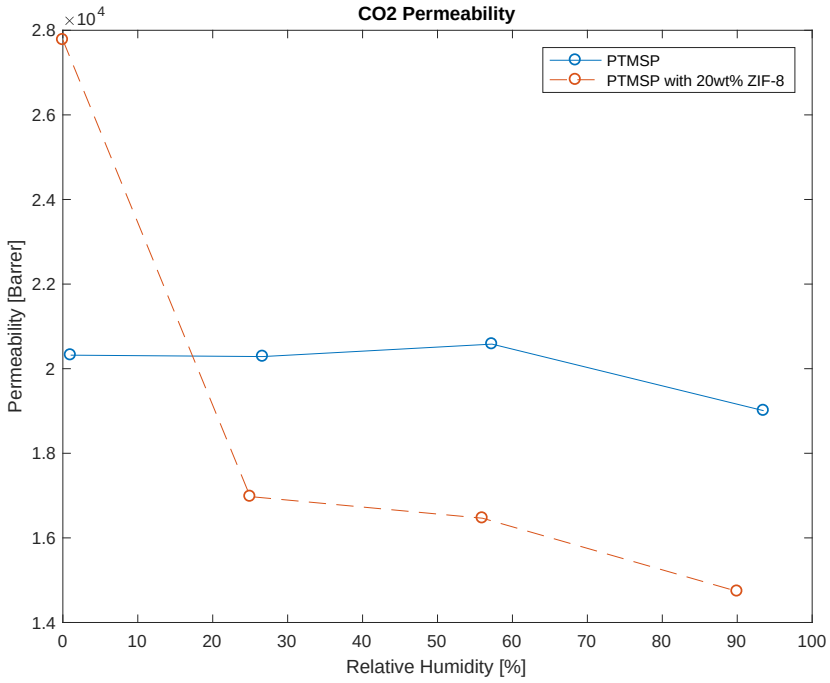

Figure 4.25: CO_2 permeability in PTMSP/ZIF-8 membranes.

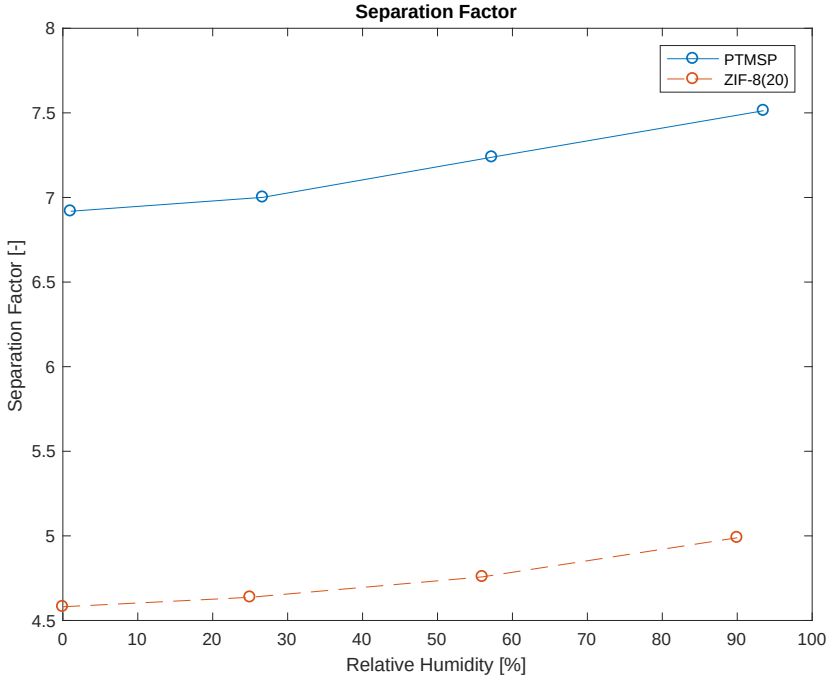

Figure 4.26: Separation factor in PTMSP/ZIF-8 membranes.

The ZIF-8(20) membrane, as well as the membranes containing ZIF-8L and TiO_2 are made using cyclohexane, and henceforth the permeation results will be compared with the appropriate results for the pure PTMSP membrane made with cyclohexane.

The separation factor for the ZIF-8(20), given by Figure 4.26 indicate that the ZIF-8 particles does not work as expected. The hypothesis was that the molecular sieving features of ZIF-8 would increase the separation between CO_2 and N_2, while the opposite is revealed to happen. The CO_2 permeability of the membrane is reported in Figure 4.25, and a great increase in permeability is observed at dry conditions (0%RH). This could be explained by poor adhesion between ZIF-8 and polymer phase, resulting in voids around the nanofillers. A sudden change is observed as the RH increase from 0% to 30%, but as this is not the fact for the separation factor, the difference is also happening for the N_2 permeability. It could be related to the particle instability in contact with moisture, as mentioned in Section 2.4. As documented with images taken by S(T)EM by another Master Student belonging to MEMFO (at Department of Chemical Engineering, NTNU), membranes containing ZIF-8 and ZIF-8L experienced major degradation after being exposed to 100% humid conditions for 1 week. Another possible explanation could be accumulation of water vapour in the voids around the ZIF-8 particles. The permeability of ZIF-8 and water are inferior to the permeability through the polymer, and thus the transport could be dominated by the polymer phase when water vapour becomes present.

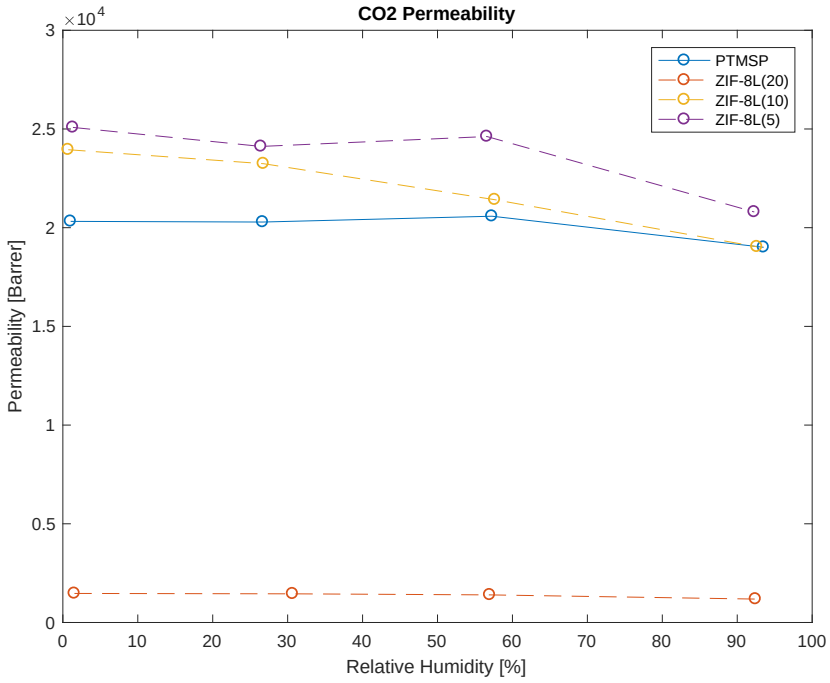

Figure 4.27: CO_2 permeability in PTMSP/ZIF-8L membranes.

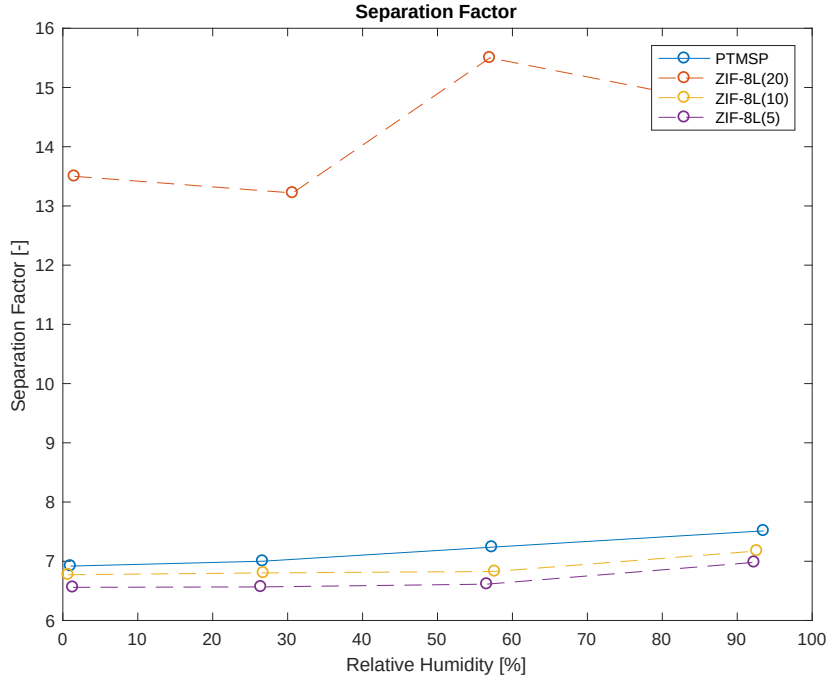

Figure 4.28: Separation factor in PTMSP/ZIF-8L membranes.

In Figure 4.27 the CO_2 permeability in the ZIF-8L blend membranes are presented. Standing out is the results for the ZIF-8L(20) membrane. A drastic decrease in permeability and a subsequent inverse response for the separation factor are revealed. ZIF-8L exhibit a quite high aspect ratio, as the particle dimensions are 5 µm x 2 µm x 150 nm. Thus, the particles might fully cover the whole membrane, resulting in the decreased permeability since the intrinsic permeability within ZIF-8L particles are much lower than in the PTMSP polymer phase, while the selectivity of the particle greatly reduce the permeability of N_2 in comparison to CO_2. By adding a small amount (5wt%) the CO_2 permeability increased by 25%. Seeing that there is close to no change in the separation factor, the N_2 permeability increased proportionally with CO_2. With a slight decrease in separation factor in relation with the increased permeability, it could be that the interface for ZIF-8L and PTMSP are not optimal in this membrane. Different from ZIF-8(20), the ZIF-8L membranes did not reveal any abnormal behaviour in contact with moisture in the feed and sweep gas streams. This could be due to the fact that the structure of ZIF-8L could be slightly more stable. The permeation tests were usually approximately 2 hours per test due to a limited amount of testing time, and if the tests had been carried out for a longer period of time, the instability of the particle might become more prominent.

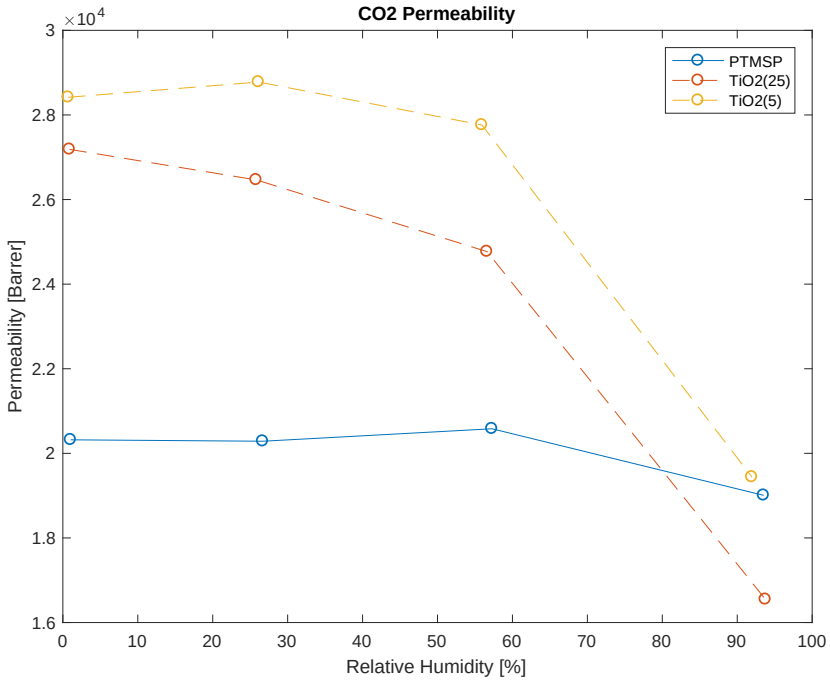

Figure 4.29: CO_2 permeability in PTMSP/TiO_2 membranes.

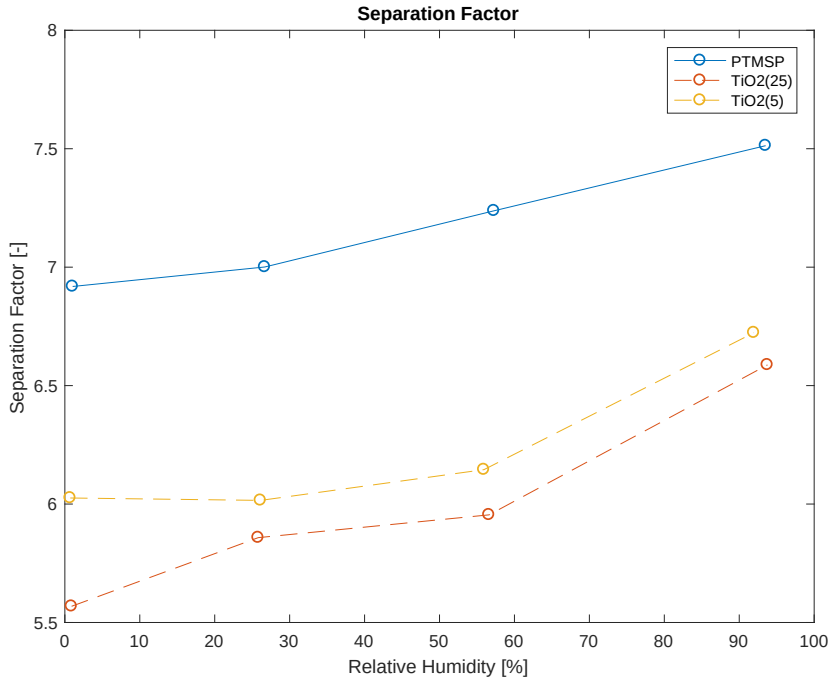

Figure 4.30: Separation factor in PTMSP/TiO_2 membranes.

For the TiO_2-membranes, presented in figures 4.29 and 4.30, there were an increase of 37% and 33% for the 5wt% and 25wt% membrane, respectively, at dry conditions. Ahn et al. (2010) state that it is difficult to distinguish the exact reason for the increased permeability, but propose two different reasons. The increase could be due to microvoids forming at the interface between nanoparticle and polymer phase, or due to a disruption of the polymer chains, leading to a higher free volume. The reduction in α with the addition of impermeable particles is also in coherence with Ahn et al. (2010), where the selectivity dropped with increasing amount of additive. The nanoparticle (TiO_2) used was reported to have hydrophilic properties, which might explain what occurs when the RH is increased to 100%. The sudden decrease in permeability could be a result of water-channels/water domains forming in the voids between polymer and nanoparticle. The permeability decreases as the gases have a slower rate of solubility and transport through the water domains, than regular diffusion throughout the polymer phase. The increase in separation factor for 100%RH could be attributed to the fact that CO_2 have a higher degree of solubility in water than that of N_2. At 25 °C the solubility for CO_2 and N_2 are 1.45 g kg^{-1} and 0.0175 g kg^{-1}, respectively (Aylward and Findlay, 2008).

Low et al. (2013) report a necessary permeance of 1000 gpu (gas permeation unit) for a membrane to be attractive for utilization, where 1 gpu corresponds to a permeability of 1 Barrer in a membrane of thickness 1 µm (Baker, 2004a). When calculating the permeance of all the testes membranes none of them reach the requirement for being technologically feasible. The permeance of the membranes are summarized in Table 4.2. Noteworthy, is that all mixed matrix membranes made with cyclohexane have an improved permeance compared to the pure polymer membrane, with the exception of ZIF-8L(20).

Table 4.2: Permeance of membranes.

Membrane	**Permeance [gpu]**
PTMSP (cyclohexane)	325
PTMSP (chloroform)	674
ZIF-7	631
ZIF-8	444
ZIF-8L(20)	15
ZIF-8L(10)	425
ZIF-8L(5)	404
TiO_2(25)	557
TiO_2(5)	519

The effect of different temperatures and pressure was not further investigated due to the membranes not performing well enough to be economically/technologically feasible with the current performance.

5 Conclusion

The object of the current Master's Thesis was to improve the separation properties of high free volume polymers, specifically PTMSP, by the addition of both porous and nonporous fillers. Mixed matrix membranes were fabricated, characterized and tested for properties related to the permeability and separation factor of the gas pair CO_2/N_2.

Specifically, the intention was to explore a new method for carbon capture by achieving superior separation properties related to the aforementioned gas pair. Three different porous fillers (ZIF-7, ZIF-8 and ZIF-8L) were utilized due to their reported preferable properties in relation to CO_2 separation. In addition, a nonporous filler (TiO_2), was investigated to obtain a better understanding of nanoparticles into PTMSP in general, since the ZIF particles all were closely related in terms of properties and size.

The thermal stability of the nanoparticles was shown to be better than that of the pure polymer PTMSP. It was thus observed that the thermal stability of the membranes increased with an increase in additive in the MMM. The experimental DSC confirmed that no glass transition temperature, T_g, was found for the polymer - with no observable difference for the MMMs.

All membranes, including the nanoparticles, were explored using FT-IR spectroscopy. The results were in accordance with literature, confirming the chemical structure of PTMSP, and the successful addition of nanoparticles into the membrane matrix.

From the cross-section SEM images, it was clear that membrane-fabrication by casting knife is by far the superior method for achieving a well dispersed mixed matrix. Overall, the nanoparticles had a good distribution, with only minor occurrence of agglomeration of particles. Some holes/voids are visible in the cross-section images, but it is difficult to determine if this is a fabrication error such as sieving cages or caused by the freeze fracturing when preparing the SEM samples.

In accordance with literature, the effect of solvent for PTMSP was found to be important. Switching from chloroform to cyclohexane improved α by 150% for the pure polymer membrane, believed to be due to a decrease in free volume within the polymer matrix. As a result, the cyclohexane PTMSP membrane came closer to the Robeson Upper Bound, but the overall permeance was reduced. The addition of nanoparticles into the membrane was done with

varying success. Of the four different nanoparticles, only ZIF-7 led to a decent increase in α, without affecting the CO_2 permeability to a higher extent, as observed in the ZIF-8L(20) membrane. Although, it should be noted that the ZIF-7(30) membrane had different casting method, solvent and nanoparticles and it might be difficult to do a direct comparison between ZIF-7(30) and the other MMMs. An issue arising especially for ZIF-8 and TiO_2 were their apparent reaction when the mixed matrix membranes came in contact with humid conditions. For membranes containing the other nanoparticles, it is believed that instability of nanoparticles (specially ZIF-8) and a poor interface between polymer and additive was the cause of the less than expected results in relation to the separation properties.

Further investigation would be required to state for certain the main reasons for the results. Seeing as PTMSP is still a highly interesting polymer, mainly due to its very high permeability, further research should be carried out to be able to fabricate economically and technologically viable membranes utilizing PTMSP. Some possibilities could be to further investigate effect of solvents, preparation method, pre-treatment of nanoparticles to improve the polymer-nanoparticle interface or addition of other promising inorganic fillers. Based on the results for permeability and permeance, one possibility could be trying to go back to chloroform and investigate if it is achievable to increase the separation factor.

References

Ahn, J., Chung, W.-J., Pinnau, I., Song, J., Du, N., Robertson, G. P., and Guiver, M. D. (2010). Gas transport behavior of mixed-matrix membranes composed of silica nanoparticles in a polymer of intrinsic microporosity (pim-1). *Journal of membrane science*, 346(2):280–287.

Ansaloni, L. (2014). *Polymeric membranes for CO_2 Separtion: Effect of Aging, Humidity and Facilitated Transport*. PhD thesis, Università de Bologna.

Ansaloni, L. and Deng, L. (2016). Advances in polymer-inorganic hybrids as membrane materials 7. *Recent Developments in Polymer Macro, Micro and Nano Blends: Preparation and Characterisation*, page 163.

Ansaloni, L. and Deng, L. (2017). 7 - advances in polymer-inorganic hybrids as membrane materials. In Visakh, P., Markovic, G., and Pasquini, D., editors, *Recent Developments in Polymer Macro, Micro and Nano Blends*, pages 163 – 206. Woodhead Publishing.

Aylward, G. and Findlay, T. (2008). *SI Chemical Data*. Wiley.

Bacsik, Z., Mink, J., and Keresztury, G. (2004). Ftir spectroscopy of the atmosphere. i. principles and methods. *Applied Spectroscopy Reviews*, 39(3):295–363.

Baker, R. W. (2004a). *Appendix*, pages 523–534. John Wiley & Sons, Ltd.

Baker, R. W. (2004b). *Gas Separation*, pages 301–353. John Wiley & Sons, Ltd.

Baker, R. W. (2004c). *Membrane Transport Theory*, pages 15–87. John Wiley & Sons, Ltd.

Baker, R. W. (2004d). *Membranes and Modules*, pages 89–160. John Wiley & Sons, Ltd.

Baker, R. W. (2004e). *Overview of Membrane Science and Technology*, pages 1–14. John Wiley & Sons, Ltd.

Baker, R. W., Wijmans, J., and Huang, Y. (2010). Permeability, permeance and selectivity: A preferred way of reporting pervaporation performance data. *Journal of Membrane Science*, 348(1–2):346 – 352.

Bazhenov, S. D., Borisov, D. S., Rybakova, A. N., Khotimskiy, V. S., Molchanov, S. P., and

Volkov, V. V. (2016). High-permeance crosslinked ptmsp thin-film composite membranes as supports for CO_2 selective layer formation.

Bi, J. J., Simon, G., Yamasaki, A., Wang, C., Kobayashi, Y., and Griesser, H. (2000). Effects of solvent in the casting of poly (1-trimethylsilyl-1-propyne) membranes. *Radiation Physics and Chemistry*, 58(5):563–566.

Bi, J. J., Wang, C., Kobayashi, Y., Ogasawara, K., and Yamasaki, A. (2003). Effect of the casting solvent on the free-volume characteristics and gas permeability of poly [1-(trimethylsilyl)-1-propyne] membranes. *Journal of applied polymer science*, 87(3):497–501.

Bradley, M. Ftir basics. `https://goo.gl/H4NrWI`. Accessed: 06.12.2016.

Budd, P. M., Ghanem, B. S., Makhseed, S., McKeown, N. B., Msayib, K. J., and Tattershall, C. E. (2004). Polymers of intrinsic microporosity (pims): robust, solution-processable, organic nanoporous materials. *Chemical Communications*, (2):230–231.

Bushell, A. F., Attfield, M. P., Mason, C. R., Budd, P. M., Yampolskii, Y., Starannikova, L., Rebrov, A., Bazzarelli, F., Bernardo, P., Jansen, J. C., et al. (2013). Gas permeation parameters of mixed matrix membranes based on the polymer of intrinsic microporosity pim-1 and the zeolitic imidazolate framework zif-8. *Journal of membrane science*, 427:48–62.

Chapala, P. P., Bermeshev, M. V., Starannikova, L. E., Belov, N. A., Ryzhikh, V. E., Shantarovich, V. P., Lakhtin, V. G., Gavrilova, N. N., Yampolskii, Y. P., and Finkelshtein, E. S. (2015). A novel, highly gas-permeable polymer representing a new class of silicon-containing polynorbornens as efficient membrane materials. *Macromolecules*, 48(22):8055–8061.

Chen, R., Yao, J., Gu, Q., Smeets, S., Baerlocher, C., Gu, H., Zhu, D., Morris, W., Yaghi, O. M., and Wang, H. (2013). A two-dimensional zeolitic imidazolate framework with a cushion-shaped cavity for co 2 adsorption. *Chemical Communications*, 49(82):9500–9502.

Consolati, G., Genco, I., Pegoraro, M., and Zanderighi, L. (1996). Positron annihilation lifetime (pal) in poly [1-(trimethyl-silyl) propine](ptmsp): Free volume determination and time dependence of permeability. *Journal of Polymer Science Part B: Polymer Physics*, 34(2):357–367.

Dai, Z., Ansaloni, L., and Deng, L. (2016). Recent advances in multi-layer composite polymeric membranes for co 2 separation: A review. *Green Energy & Environment*.

Deng, L., Kim, T.-J., and Hägg, M.-B. (2009). Facilitated transport of co 2 in novel pvam/pva blend membrane. *Journal of Membrane Science*, 340(1):154–163.

Falkowski, P., Scholes, R., Boyle, E., Canadell, J., Canfield, D., Elser, J., Gruber, N., Hibbard, K., Högberg, P., Linder, S., et al. (2000). The global carbon cycle: a test of our knowledge of earth as a system. *science*, 290(5490):291–296.

Flammersheim, H., Hemminger, W., and Höhne, G. (2003). Differential scanning calorimetry.

Freeman, B. D. (1999). Basis of permeability/selectivity tradeoff relations in polymeric gas separation membranes. *Macromolecules*, 32(2):375–380.

Gibbins, J. and Chalmers, H. (2008). Carbon capture and storage. *Energy Policy*, 36(12):4317–4322.

Gooch, J. W. (2007). *Encyclopedic Dictionary of Polymers*. Springer New York.

Hägg, M.-B. and Deng, L. (2015). Membranes in gas separation. In *Handbook of Membrane Separations: Chemical, Pharmaceutical, Food, and Biotechnological Applications, Second Edition*, pages 143–180. CRC Press.

Hu, Y., Kazemian, H., Rohani, S., Huang, Y., and Song, Y. (2011). In situ high pressure study of zif-8 by ftir spectroscopy. *Chemical Communications*, 47(47):12694–12696.

Kang, C.-H., Lin, Y.-F., Huang, Y.-S., Tung, K.-L., Chang, K.-S., Chen, J.-T., Hung, W.-S., Lee, K.-R., and Lai, J.-Y. (2013). Synthesis of zif-7/chitosan mixed-matrix membranes with improved separation performance of water/ethanol mixtures. *Journal of membrane science*, 438:105–111.

Li, T., Pan, Y., Peinemann, K.-V., and Lai, Z. (2013). Carbon dioxide selective mixed matrix composite membrane containing zif-7 nano-fillers. *Journal of membrane science*, 425:235–242.

Li, Y., Liang, F., Bux, H., Yang, W., and Caro, J. (2010). Zeolitic imidazolate framework zif-7 based molecular sieve membrane for hydrogen separation. *Journal of Membrane Science*, 354(1):48–54.

Lin, W.-H. and Chung, T.-S. (2001). Gas permeability, diffusivity, solubility, and aging characteristics of 6fda-durene polyimide membranes. *Journal of Membrane Science*, 186(2):183–193.

Liu, Q., Low, Z.-X., Feng, Y., Leong, S., Zhong, Z., Yao, J., Hapgood, K., and Wang, H. (2014). Direct conversion of two-dimensional zif-l film to porous zno nano-sheet film and its performance as photoanode in dye-sensitized solar cell. *Microporous and Mesoporous Materials*, 194:1–7.

Low, B. T., Zhao, L., Merkel, T. C., Weber, M., and Stolten, D. (2013). A parametric study of the impact of membrane materials and process operating conditions on carbon capture from humidified flue gas. *Journal of membrane science*, 431:139–155.

Løining, V. S. (2016). Amine-modified high free volume polymer for gas separation. Specialization Project as Part of a MSc in Chemical Engineering at Department for Chemical Engineering, NTNU.

Mahajan, R., Koros, W., and Thundyil, M. (1999). Mixed matrix membranes: Important and challenging! *Membrane Technology*, 1999(105):6–8.

Metz, B., Davidson, O., De Coninck, H., Loos, M., Meyer, L., et al. (2005). Carbon dioxide capture and storage.

Murashkevich, A., Lavitskaya, A., Barannikova, T., and Zharskii, I. (2008). Infrared absorption spectra and structure of tio 2-sio 2 composites. *Journal of Applied Spectroscopy*, 75(5):730–734.

Nagai, K., Masuda, T., Nakagawa, T., Freeman, B. D., and Pinnau, I. (2001). Poly [1-(trimethylsilyl)-1-propyne] and related polymers: synthesis, properties and functions. *Progress in Polymer Science*, 26(5):721–798.

Painter, P. C. and Coleman, M. M. (1997). *Fundamentals of polymer science: an introductory text*. CRC Press LLC, 2 edition. Pages 290-292.

Raade, G. (2009). Termogravimetri. `https://snl.no/termogravimetri`. Accessed: 14.11.2016.

Robeson, L. M. (2008). The upper bound revisited. *Journal of Membrane Science*, 320(1):390–400.

Seglem, K. N. (2017). *Development of membrane materials for a membrane contactor*. PhD thesis, Norwegian University of Science and Technology.

Shao, L., Liu, L., Cheng, S.-X., Huang, Y.-D., and Ma, J. (2008). Comparison of diamino cross-linking in different polyimide solutions and membranes by precipitation observation and gas transport. *Journal of Membrane Science*, 312(1):174–185.

Srinivasan, R., Auvil, S., and Burban, P. (1994). Elucidating the mechanism (s) of gas transport in poly [1-(trimethylsilyl)-1-propyne](ptmsp) membranes. *Journal of Membrane Science*, 86(1):67–86.

Vatanpour, V., Madaeni, S. S., Khataee, A. R., Salehi, E., Zinadini, S., and Monfared, H. A. (2012). Tio 2 embedded mixed matrix pes nanocomposite membranes: influence of different sizes and types of nanoparticles on antifouling and performance. *Desalination*, 292:19–29.

Wang, W., Yung, Y., Lacis, A., Mo, T. a., and Hansen, J. (1976). Greenhouse effects due to man-made perturbations of trace gases. *Science*, 194(4266):685–690.

Wang, X.-Y., Lee, K. M., Lu, Y., Stone, M. T., Sanchez, I., and Freeman, B. (2004). Cavity size distributions in high free volume glassy polymers by molecular simulation. *Polymer*, 45(11):3907–3912.

Yang, T., Xiao, Y., and Chung, T.-S. (2011). Poly-/metal-benzimidazole nano-composite membranes for hydrogen purification. *Energy & Environmental Science*, 4(10):4171–4180.

Zhang, C., Dai, Y., Johnson, J. R., Karvan, O., and Koros, W. J. (2012). High performance zif-8/6fda-dam mixed matrix membrane for propylene/propane separations. *Journal of Membrane Science*, 389:34–42.

Zhang, H., Liu, D., Yao, Y., Zhang, B., and Lin, Y. (2015). Stability of zif-8 membranes and crystalline powders in water at room temperature. *Journal of Membrane Science*, 485:103–111.

Zhang, W., Hu, Y., Ge, J., Jiang, H.-L., and Yu, S.-H. (2014). A facile and general coating approach to moisture/water-resistant metal–organic frameworks with intact porosity. *Journal of the American Chemical Society*, 136(49):16978–16981.

Zhong, Z., Yao, J., Chen, R., Low, Z., He, M., Liu, J. Z., and Wang, H. (2015). Oriented

two-dimensional zeolitic imidazolate framework-l membranes and their gas permeation properties. *Journal of Materials Chemistry A*, 3(30):15715–15722.

A PTMSP Membranes

Figures A.1-A.4 display several unused membranes, some of which turned out quite bad due to incorrect evaporation rate. In Figure A.5 display the ZIF-8L(5) membrane, which has been used for different experimental tests.

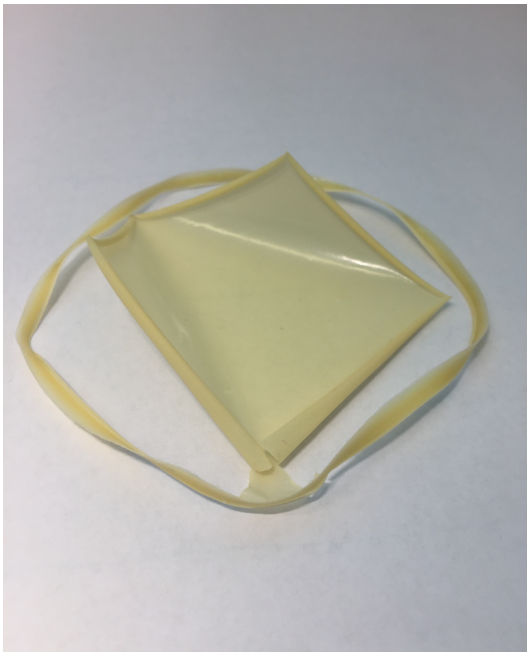

Figure A.1: PTMSP/ZIF-8 membrane cast in Petri dish.

Figure A.2: PTMSP/ZIF-8L membrane cast in Petri dish.

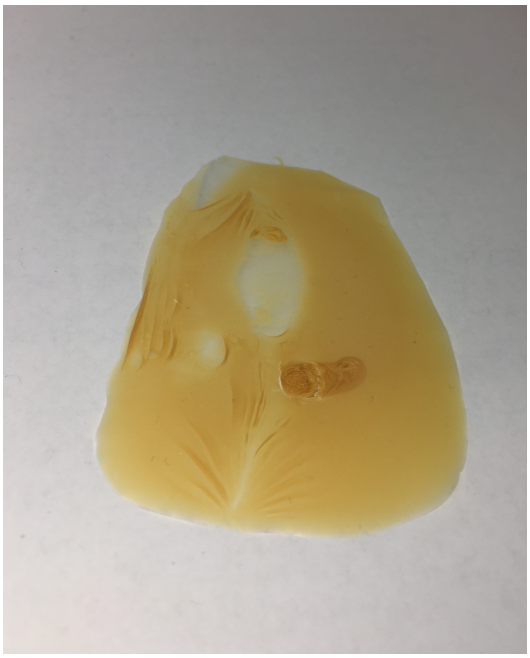

Figure A.3: PTMSP/ZIF-8 membrane made with casting knife.

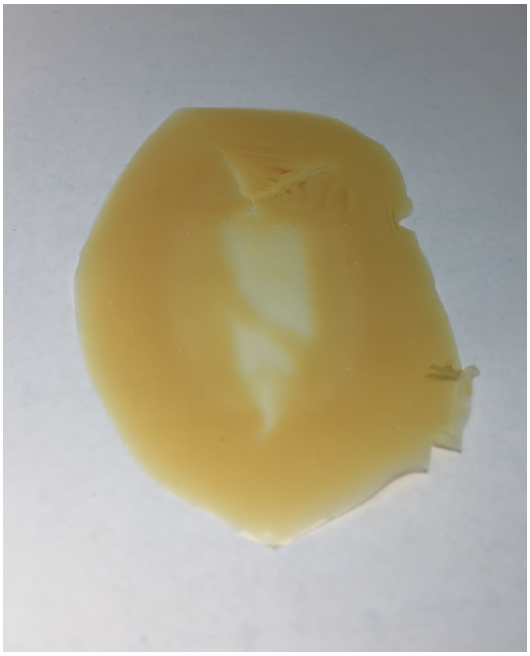

Figure A.4: PTMSP/ZIF-8 membrane made with casting knife.

Figure A.5: PTMSP/ZIF-8L membrane made with casting knife.

B PI Membrane Data

Figure B.1 display the FT-IR spectra of PI.

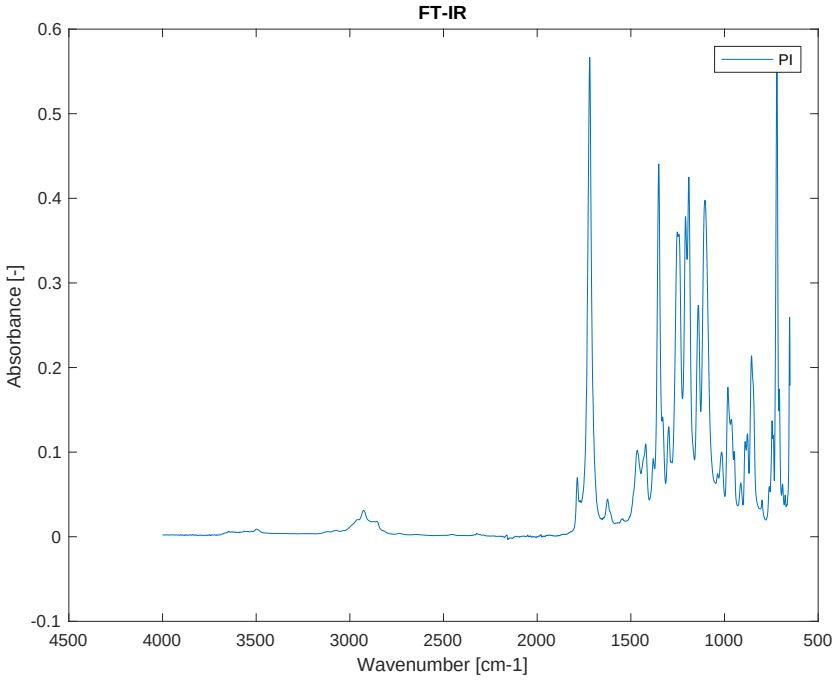

Figure B.1: FT-IR of pure PI.

Figures B.2-B.5 and present SEM surface images of PI and different PI/ZIF-8L membranes.

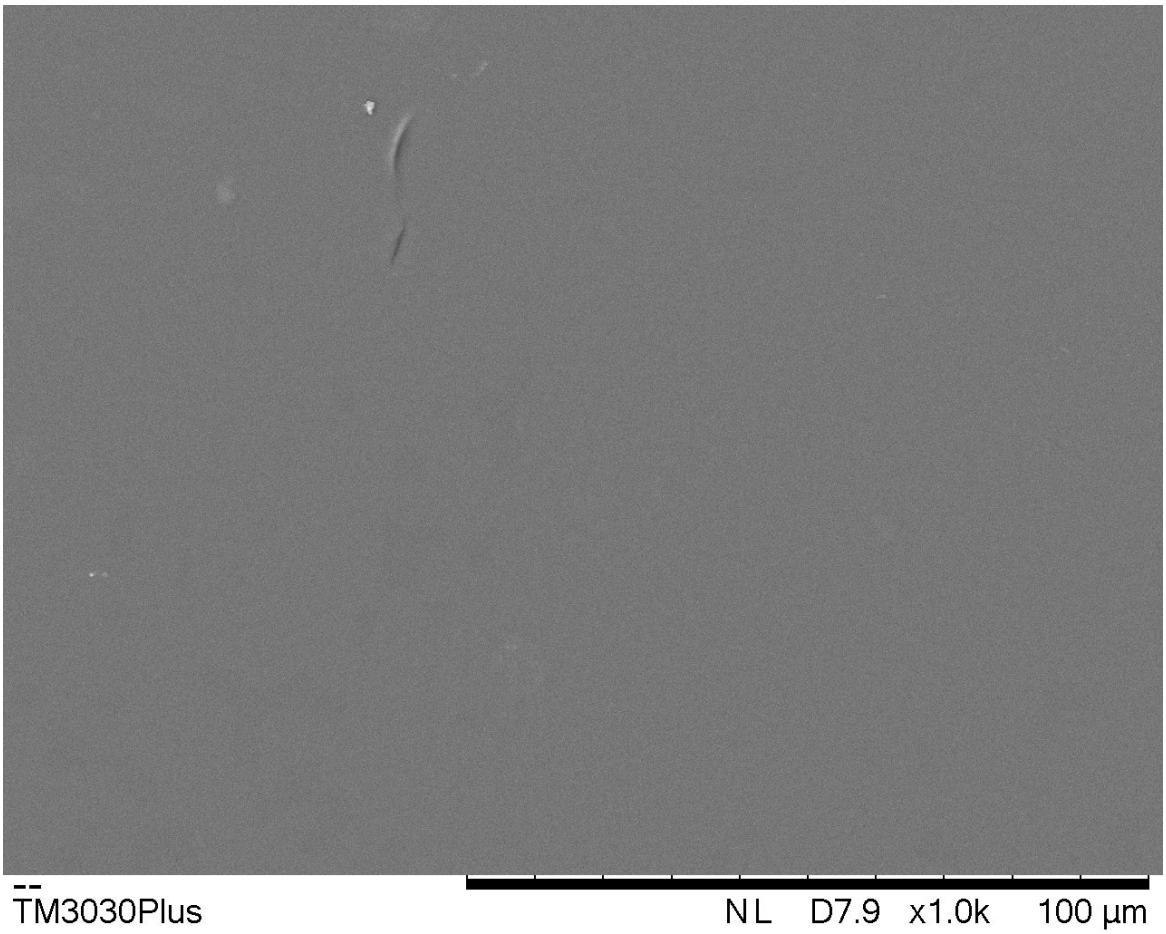

Figure B.2: SEM surface image of PI.

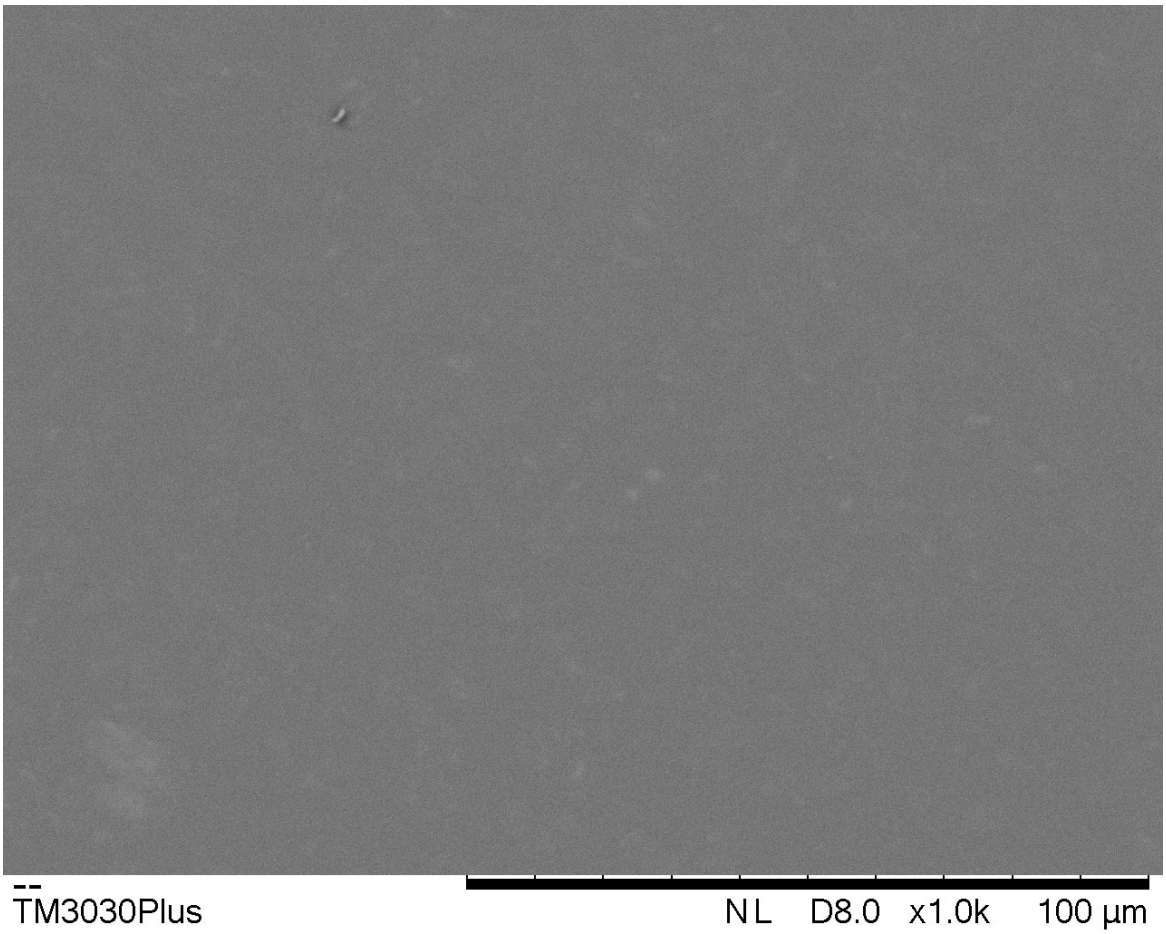

Figure B.3: SEM surface image of PI/2wt%ZIF-8L.

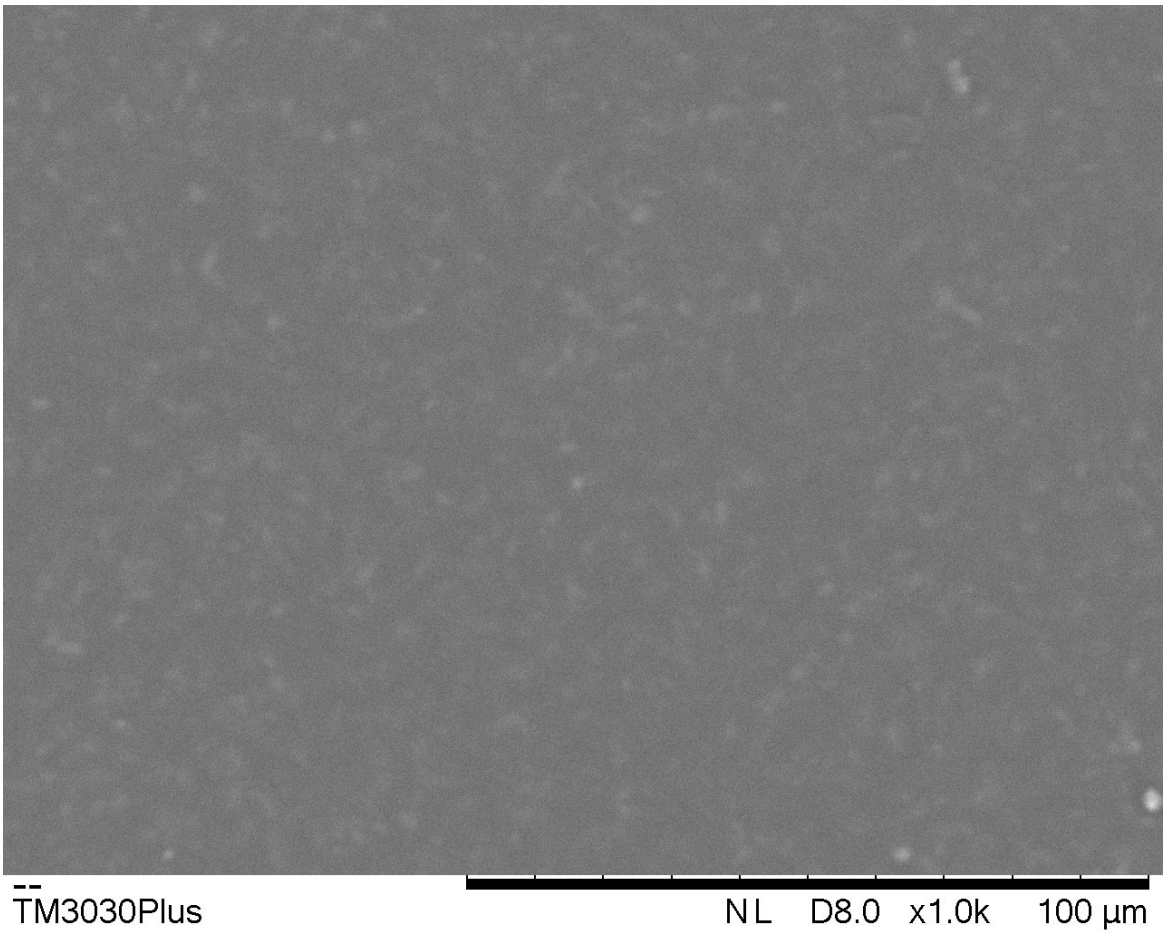

Figure B.4: SEM surface image of PI/4wt%ZIF-8L.

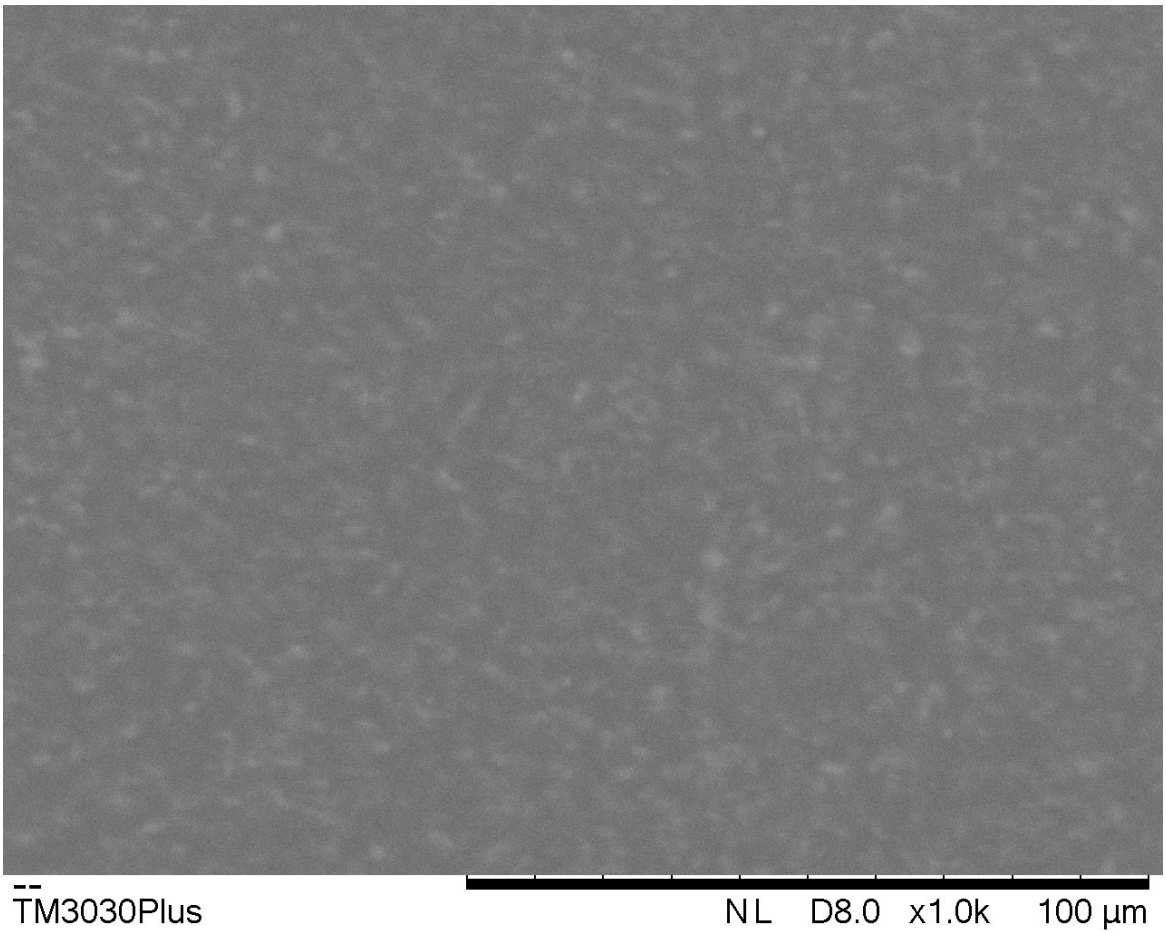

Figure B.5: SEM surface image of PI/10wt%ZIF-8L.

C DSC Results

The following figures (C.1-C.4) present the data from DSC, in the temperaturerange [25-300°C] just to confirm that no T_g is present in the given range.

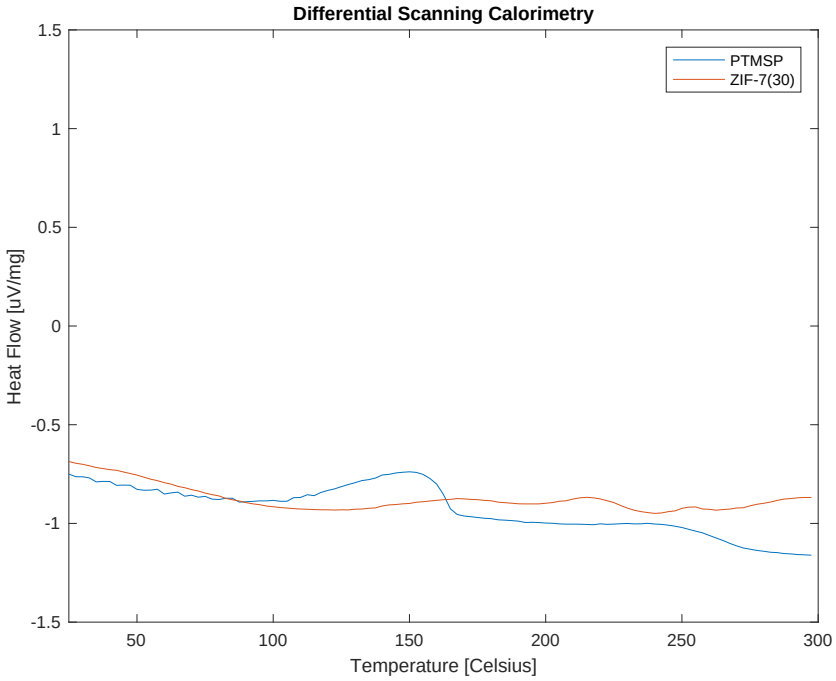

Figure C.1: Differential Scanning Calorimetry of PTMSP/ZIF-7 membranes.

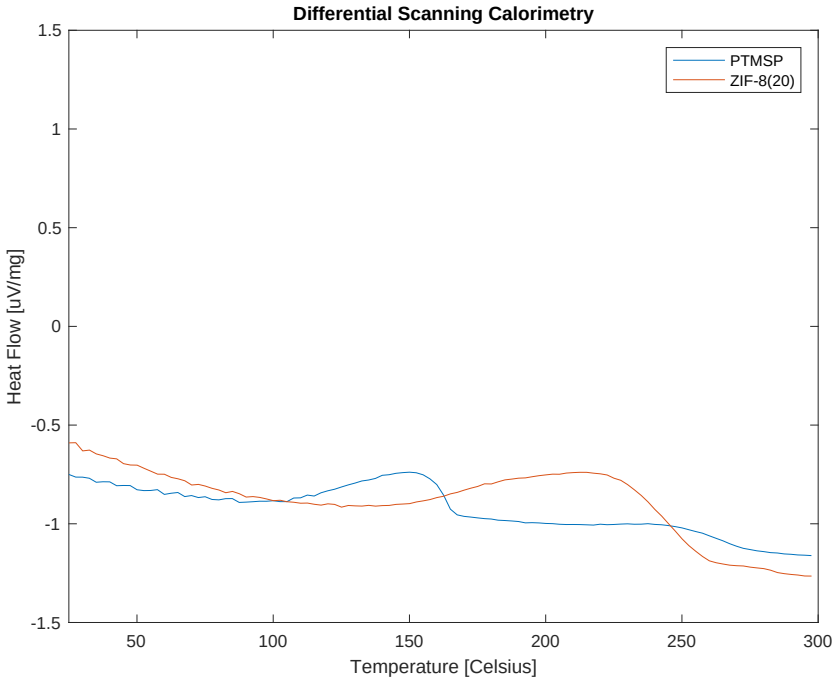

Figure C.2: Differential Scanning Calorimetry of PTMSP/ZIF-8 membranes.

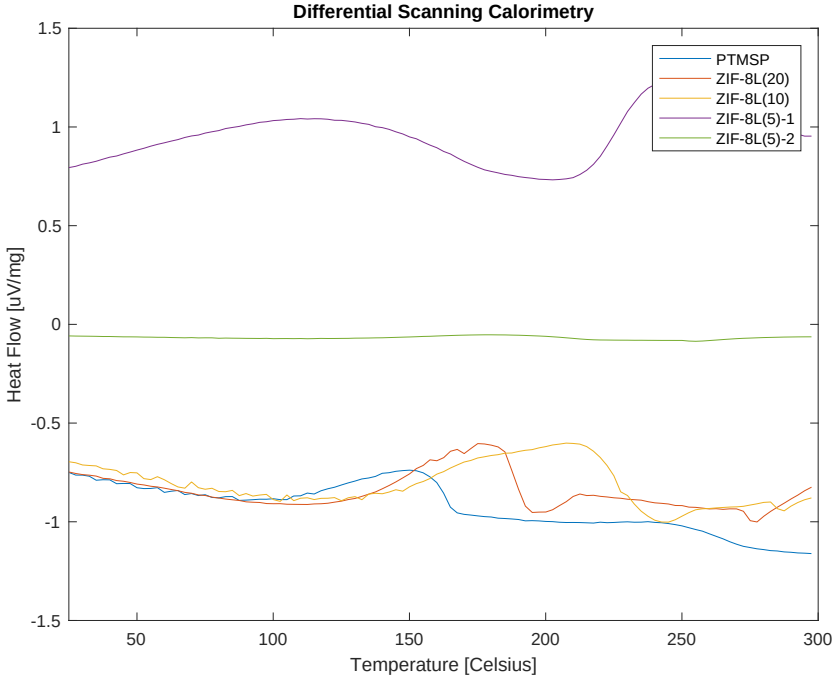

Figure C.3: Differential Scanning Calorimetry of PTMSP/ZIF-8L membranes.

The behaviour of ZIF-8L(5) is deviating from the other samples in two different tests.

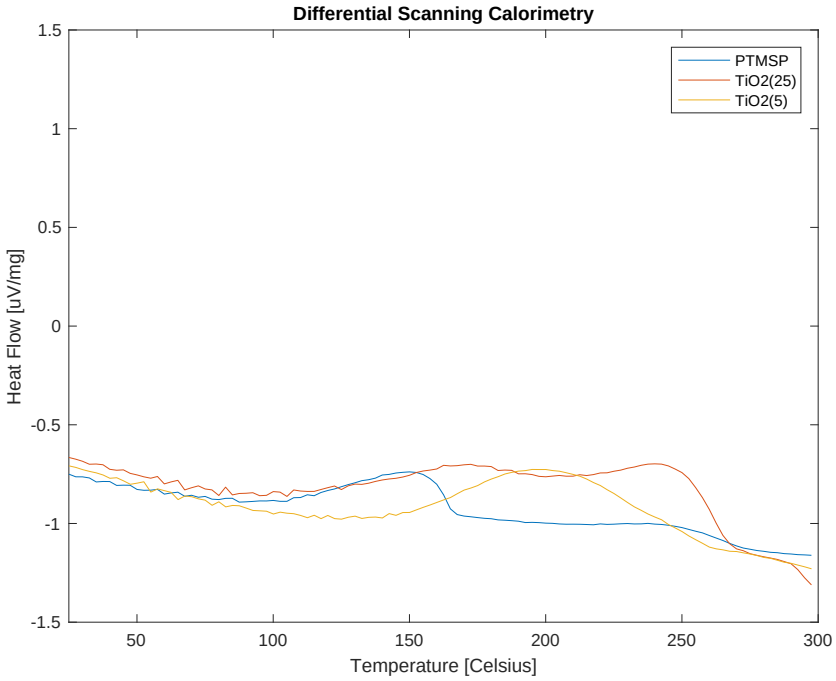

Figure C.4: Differential Scanning Calorimetry of PTMSP/TiO_2 membranes.

D FT-IR Results

The following figures, D.1-D.4, give the full spectrum for the FT-IR spectroscopy.

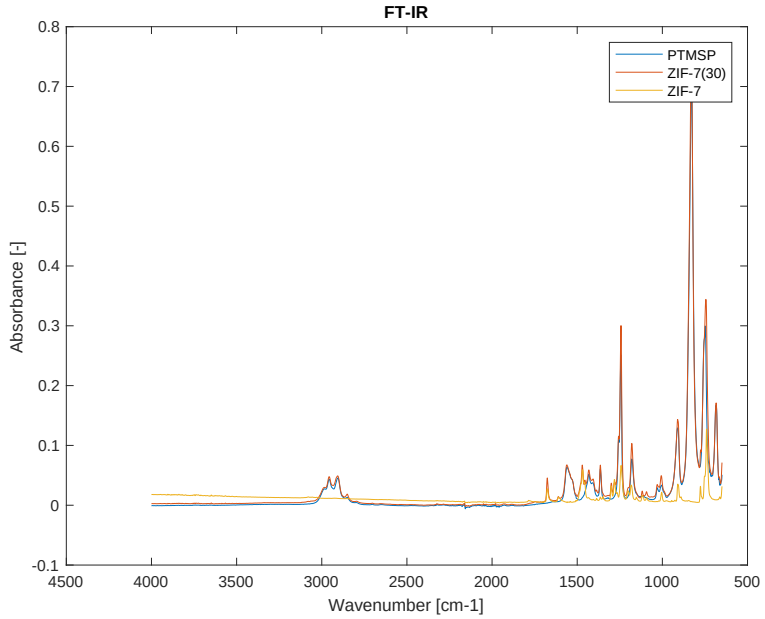

Figure D.1: Full FT-IR spectrum of PTMSP/ZIF-7 membranes and ZIF-7 nanoparticles.

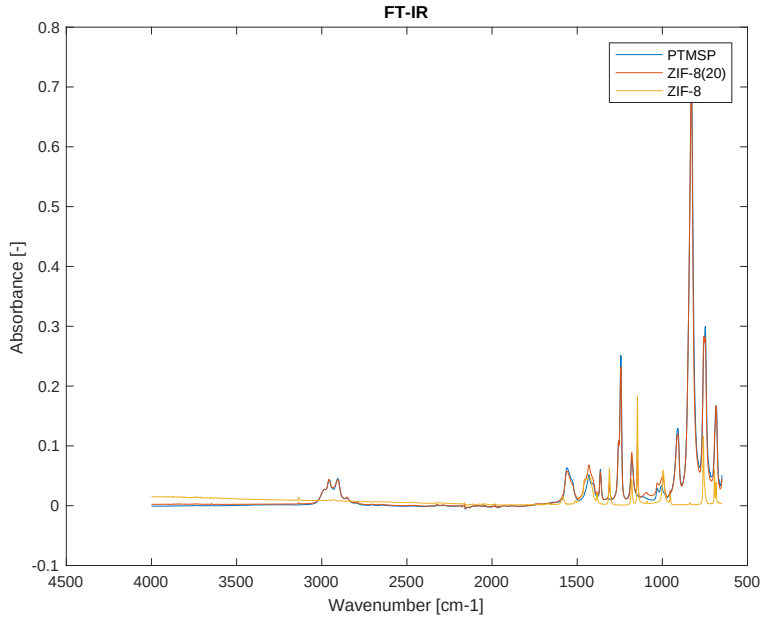

Figure D.2: Full FT-IR spectrum of PTMSP/ZIF-8 membranes and ZIF-8 nanoparticles.

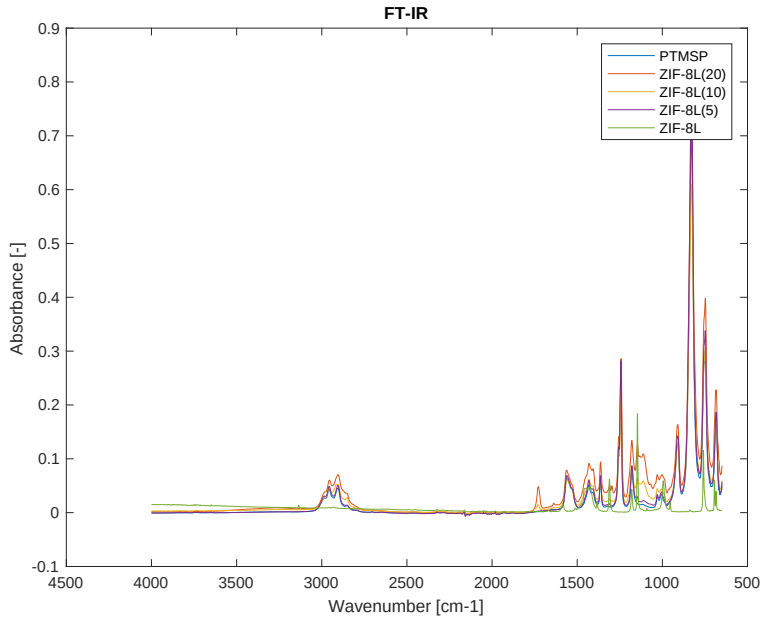

Figure D.3: Full FT-IR spectrum of PTMSP/ZIF-8L membranes and ZIF-8L nanoparticles.

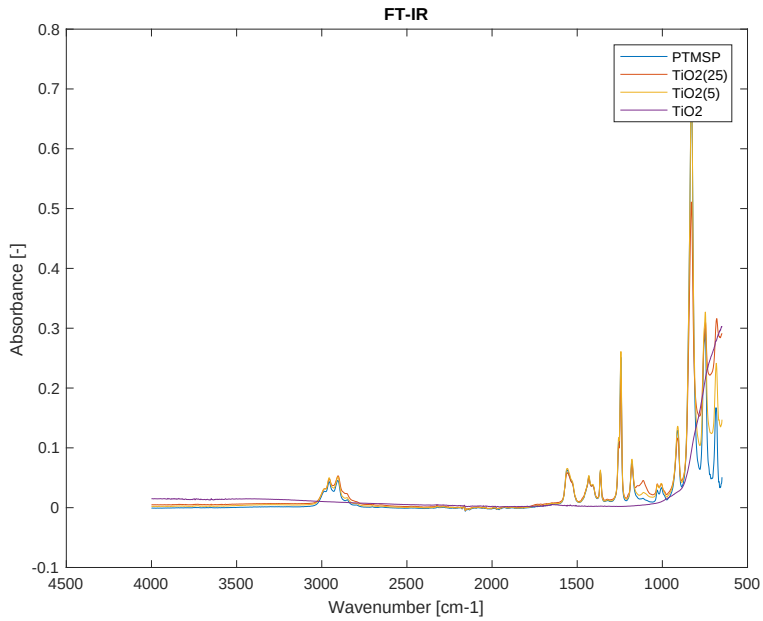

Figure D.4: Full FT-IR spectrum of PTMSP/TiO_2 membranes and TiO_2 nanoparticles.

E Additional Permeability Data

The permeability and separation factor at dry conditions (0%RH) are given in Table E.1. N_2 permeability is presented in figures E.1-E.5.

Table E.1: Summary of permeability at dry conditions.

Membrane	**CO_2 Permeability** [Barrer]	**Separation Factor** [-]
PTMSP	20320	6.92
PTMSP($CHCl_3$)	33165	2.73
ZIF-7(30)	32059	5.2
ZIF-8(20)	27772	4.58
ZIF-8L(20)	1471	13.5
ZIF-8L(10)	23950	6.77
ZIF-8L(5)	25079	6.56
TiO_2(25)	27186	5.57
TiO_2(5)	28418	6.03

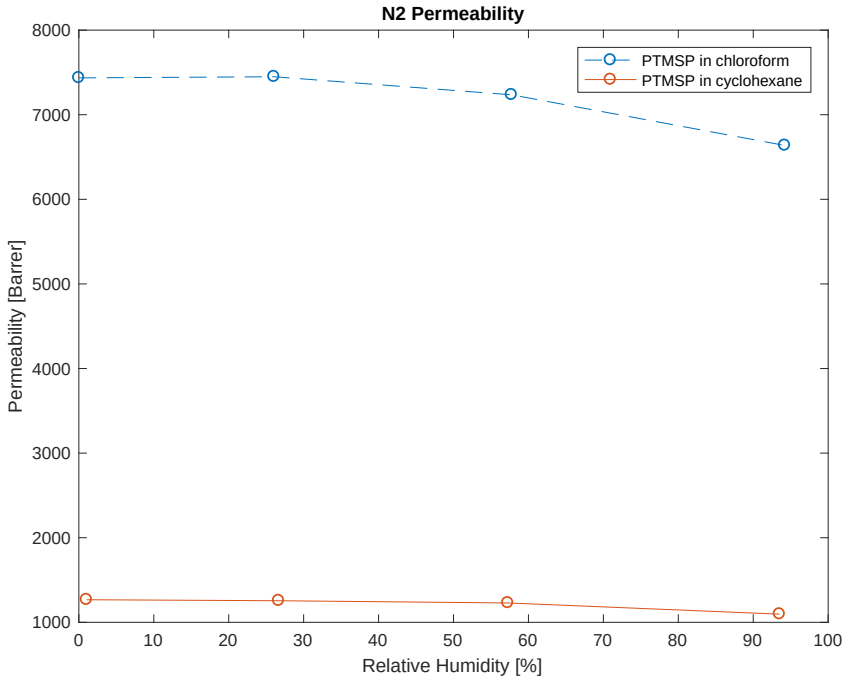

Figure E.1: N_2 permeability in pure PTMSP membranes.

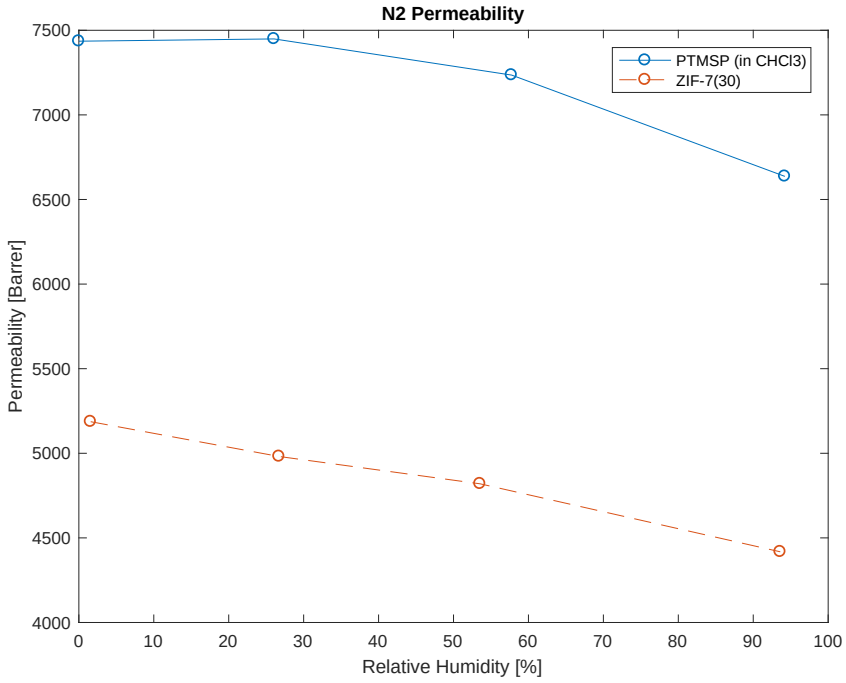

Figure E.2: N_2 permeability in PTMSP/ZIF-7 membranes.

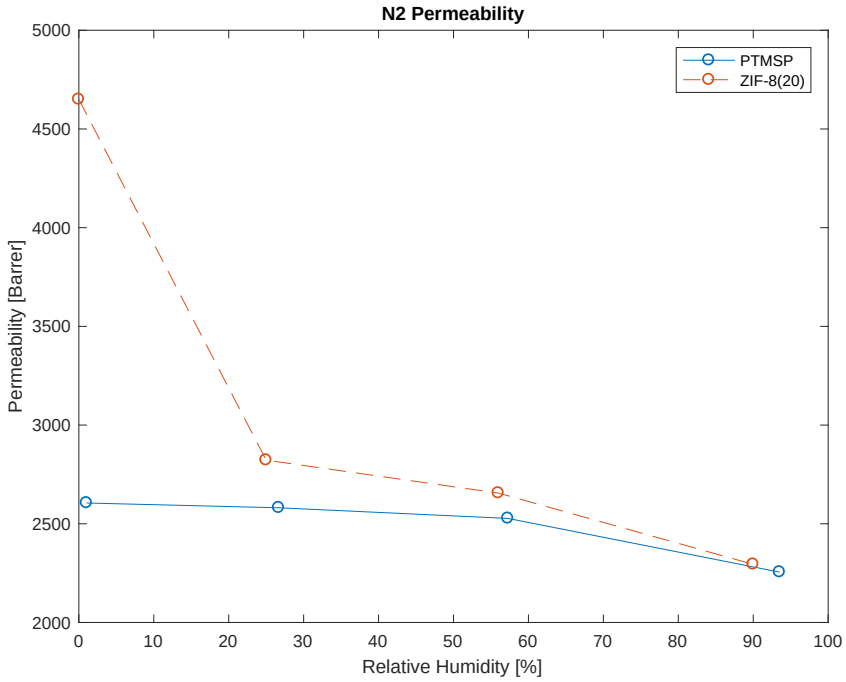

Figure E.3: N_2 permeability in PTMSP/ZIF-8 membranes.

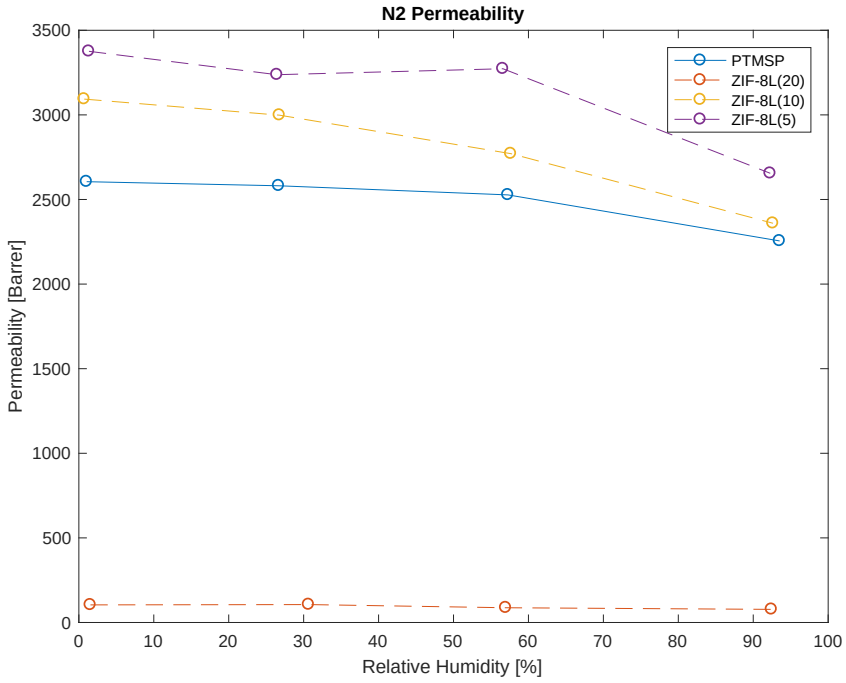

Figure E.4: N_2 permeability in PTMSP/ZIF-8L membranes.

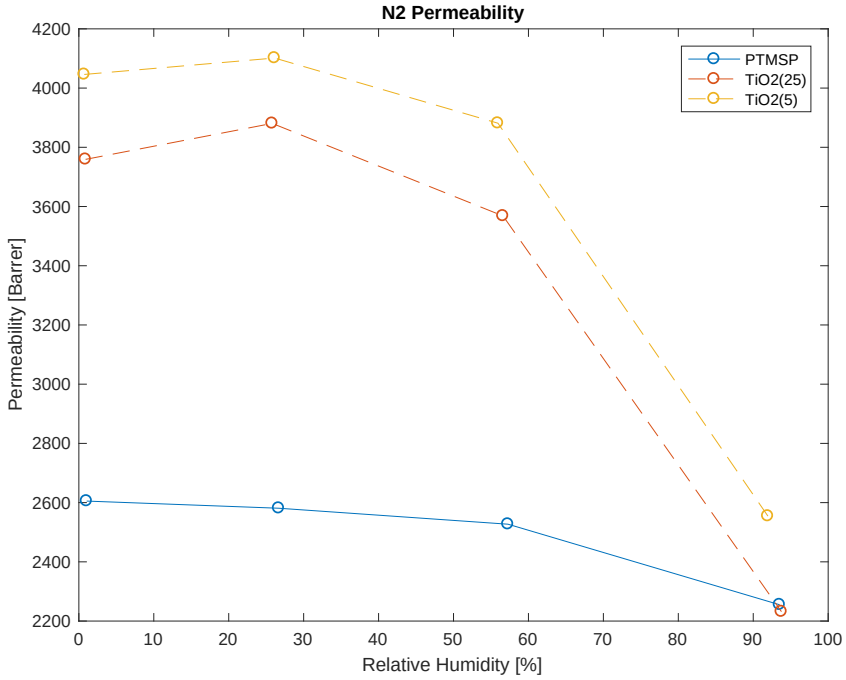

Figure E.5: N_2 permeability in PTMSP/TiO_2 membranes.